IEEE Xplore® Digital Library
http://ieeexplore.ieee.org/Xplore

Index-Domain Division Multiple Access for IoT Applications

Tengjiao Wang, *Student Member, IEEE,* Fang Yang, *Senior Member, IEEE,*
Changyong Pan, *Senior Member, IEEE,* Jian Song, *Fellow, IEEE,* and Zhu Han, *Fellow, IEEE*

***Abstract*—Facing the worldwide explosive growth of the wireless devices, the future wireless network is required to provide seamless access for the users with diverse quality of service (QoS) requirements. In this paper, a novel multiple access scheme based on the principle of multi-domain index modulation is proposed to address the downlink multiple access problem for users with diverse QoS requirements, including the Internet of Things (IoT) devices and the smart electronic devices. Unlike the conventional non-orthogonal multiple access schemes which utilize power-domain diversities to realize multiple access, in the proposed scheme, information for different users is conveyed by different domains of the transmitted signals, including the constellation domain, frequency domain, time domain, and spatial domain. As a result, the intra-cluster interference among users is alleviated and the successive interference cancellation is avoided to reduce the computational complexity of signal detection at the receiver side, which is well-suited for the IoT devices. The closed form lower bounds and approximations of the achievable rate of the proposed scheme are further derived to provide accurate estimation of the achievable rate of the communication system. Simulation results validate the superior performance of the proposed scheme over the conventional orthogonal and non-orthogonal multiple access schemes.**

***Index Terms*—Internet of Things, multiple access, multi-domain index modulation, quality of service.**

I. Introduction

In recent years, the Internet of Things (IoT) is rapidly spreading and has found its application in many areas, including smart cities [1], vehicle networks [2], and social networks [3]. In the future, it is predicted that the number of wireless communication devices will reach 28 billion by 2021 [4]. The quality of service (QoS) of the users will be much more diverse as well. Therefore, the future wireless communication networks are required to provide seamless access for the users with diverse QoS requirements [5]. The IoT devices with low data rate requirements and limited computing capabilities, and smart electronic devices with high data rate requirements and sufficient computing resources are typical users for the massive machine type communication (mMTC) and enhanced mobile broadband (eMBB) scenarios in the 5G communication systems [6]. These two kinds of users will still play important roles in the future beyond 5G networks [7], [8], and the design of efficient multiple access strategies for these users will be important enabling technologies for the future IoT networks.

The motivation of this paper is to address the multiple access problem for both the IoT devices and the smart electronic devices in the future beyond 5G networks. In this paper, a novel multiple access scheme called index-domain division multiple access (IDDMA) is proposed, which can support both the IoT devices and smart electronic devices within a single network simultaneously. This will further enhance the number of connections and coverage of IoT applications. Based on the principle of multi-domain index modulation (IM) techniques [9], the information for different users is conveyed by the multi-domain symbols to alleviate the intra-cluster interference and to avoid the use of complicated detection algorithms at the receivers. This is well-suited for the IoT devices with limited computational capacities, and low-power processors can be installed at the IoT devices to reduce power consumption. Numerical results demonstrate that the proposed IDDMA scheme can significantly reduce the detection complexity and improve the sum achievable rate.

The innovation and contribution of this paper can be summarized as follows.

- Based on the principle of multi-domain IM, a novel IDDMA framework is proposed for the future wireless communication system, which enables flexible multiple access among high-speed smart electronic devices and low-speed IoT devices. It can support both the IoT applications and mobile broadband applications within a single network simultaneously. The proposed framework and its special cases can be easily deployed in the widely used wireless communication systems, such as the multiple-input multiple-output (MIMO) system and the orthogonal frequency-division multiplexing (OFDM) system.
- Corresponding low-complexity detectors are proposed to detect the transmitted signals, which is more acceptable for the IoT users with limited computational capacities. In the proposed IDDMA framework, the information for different users are conveyed by the constellation-domain, frequency-domain, spatial-domain, and time-

This work was supported in part by the National Key Research and Development Program of China under Grant 2017YFB0403402, in part by the Guoqiang Institute of Tsinghua University, in part by the Fok Ying Tung Education Foundation, in part by NSF EARS-1839818, CNS1717454, CNS-1731424, and CNS-1702850. *(Corresponding author: Fang Yang.)*

Tengjiao Wang, Fang Yang, Changyong Pan, and Jian Song are with the Department of Electronic Engineering, Beijing National Research Center for Information Science and Technology (BNRist), Tsinghua University, Beijing 100084, P. R. China, and also with the Key Laboratory of Digital TV System of Guangdong Province and Shenzhen City, Research Institute of Tsinghua University in Shenzhen, Shenzhen 518057, P. R. China (e-mail: wangtj16@mails.tsinghua.edu.cn; fangyang@tsinghua.edu.cn; pcy@tsinghua.edu.cn; jsong@tsinghua.edu.cn).

Zhu Han is with the Department of Electrical and Computer Engineering in the University of Houston, Houston, TX 77004 USA, and also with the Department of Computer Science and Engineering, Kyung Hee University, Seoul, South Korea, 446-701 (e-mail: zhan2@uh.edu).

Digital Object Identifier: 10.1109/JIOT.2021.3055828

2327-4662 © 2021 IEEE. Personal use is permitted, but republication/redistribution requires IEEE permission.
See http://www.ieee.org/publications_standards/publications/rights/index.html for more information.

domain symbols. Therefore, the intra-cluster interference is alleviated and the complicated detection algorithms are avoided at the receivers. Thus, low-power processors can be installed at the IoT devices to reduce power consumption.

- Theoretical analyses and simulation validation are conducted. Based on the mutual information analysis, closed form lower bounds and approximations of the achievable rate of the proposed IDDMA scheme are derived to provide accurate estimation of the achievable rate of the communication system. Simulation results validate the superior bit error rate (BER) performance and reduced complexity of the proposed scheme.

The rest of this paper is organized as follows. In Section II, the related works are introduced. In Section III, the system model is briefly described. Section IV focuses on the proposed IDDMA schemes, where the frameworks of the transmitter and the receiver are explained in detail. In Section V, the performance of the proposed scheme is evaluated. Then, simulation results and discussions are provided in Section VI. Finally, the paper is concluded in Section VII.

Notation: We use the lowercase and uppercase boldface letters to denote column vectors and matrices; Transposition, conjugate transposition, inverse, and pseudo inverse are denoted by $(\cdot)'$, $(\cdot)^{\mathrm{H}}$, $(\cdot)^{-1}$, and $(\cdot)^{\dagger}$, respectively; Determinant of a matrix and Frobenius norm of a vector/matrix are denoted by $|\cdot|$ and $\|\cdot\|_{\mathrm{F}}$, respectively; Finally, $\binom{\cdot}{\cdot}$ and $\otimes$ stand for the binomial coefficient and convolution operation.

II. Related Works

In the literature, lots of multiple access techniques have been proposed, which can be divided into the orthogonal multiple access (OMA) techniques and the non-orthogonal multiple access (NOMA) techniques [10]. Unlike OMA techniques which employ orthogonal resource distribution, NOMA allocates non-orthogonal resources to different users to improve the system throughput. So far, several NOMA schemes have been investigated, which can be divided into two categories [10], the power-domain NOMA and the code-domain NOMA. The power-domain NOMA utilizes power-domain diversities to realize multiple access [11]. The code-domain one achieves multiplexing in the code domain, including the low-density spreading CDMA (LDS-CDMA) [12], the sparse code multiple access (SCMA) [13], and so on. In power-domain NOMA, successive interference cancellation (SIC) is widely used at the receiver side to enable robust signal detection. However, with a large number of users, the utilization of SIC involves high computing complexity, which is not friendly to the IoT users with limited computing capacities and power supplies.

In order to improve the energy efficiency of the communication systems, the concept of IM has been proposed recently [9]. Unlike conventional modulation schemes, only a fraction of certain indexed resources are activated for data transmission and others are kept unused [9]. The information bits can be conveyed by not only the ordinary amplitude phase modulation (APM) symbols, but also the indices of the activated resources. Therefore, IM is capable of achieving similar throughput as its conventional non-IM counterpart with reduced complexity and energy consumption [9]. Various IM schemes have been proposed and the dominated schemes can be classified into three categories according to the manipulated signal domains, including time-domain IM [14], [15], spatial-domain IM [16], [17], and frequency-domain IM [18], [19], where the indexed resources are time slots, transmit antennas, and subcarriers, respectively. Various multi-domain IM techniques have been adopted in diverse communication networks, including the mmWave communication systems [20], massive MIMO systems [21], and visible light communication systems [22]. Therefore, IM techniques are able to be incorporated with other key techniques in the future communication networks.

So far, many efforts have been made to combine the IM techniques with the NOMA techniques in order to improve the performance of the wireless communication systems. In [23], the authors proposed a NOMA-based spatial-domain IM scheme by introducing the concept of spatial-domain IM to power-domain NOMA to achieve a trade-off between spectral efficiency and interference mitigation. In [24], a transmission scheme was proposed by cooperating spatial-domain IM and power-domain NOMA, and the achievable spectral efficiency of the proposed scheme is further analyzed through mutual information analyses. A similar idea combining spatial-domain IM and power-domain NOMA was proposed in [25], where the pre-coding procedure is involved. However, because of power-domain superposition coding, the SIC detections with high computational complexity are necessary in these schemes, which cannot be tolerated by the users with limited computational capabilities, especially when more users are supported. Moreover, users' QoSs are not taken into consideration, which limit the efficiency of resource allocations. In order to reduce the computational complexity at the receiver, novel spatial-domain IM aided NOMA schemes have been proposed in [26] and [27] by modulating the information for different users on ordinary APM symbols and indices of activated antennas, respectively. In [28], a novel frequency-domain index modulation aided multiple access scheme has been proposed for the optical wireless communication system, by modulating the information for different users on APM symbols and indices of the activated subcarriers. However, since only single-domain IM technique is taken into consideration in [26], [27] and [28], only two users can be supported in each user cluster, which limits the user capacity and flexibility of the multiple access strategies.

III. System Model

In this section, the basic system models of the widely employed wireless communication systems and various IM techniques in multiple domains are briefly introduced. The single-input single-output (SISO) system with time-domain IM, the MIMO system with spatial-domain IM, and the OFDM system with frequency-domain IM are introduced in Section III-A, Section III-B, and Section III-C, respectively. Illustrations of the multi-domain IM techniques are also provided in Fig. 1.

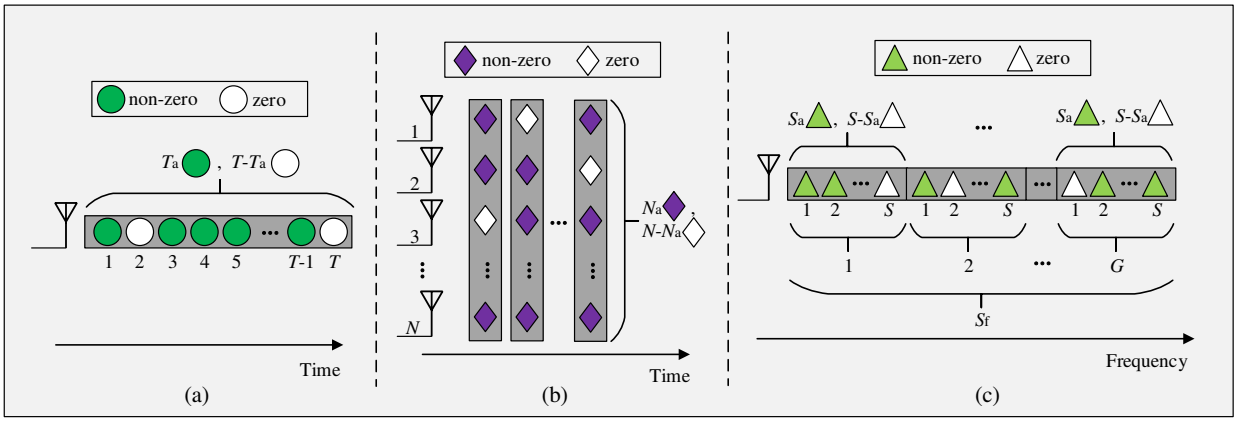


Fig. 1. Illustrations of the multi-domain IM techniques: a) time-domain IM; b) spatial-domain IM; c) frequency-domain IM.

A. SISO System with Time-Domain IM

SISO format is the most straightforward wireless communication system. Only one transmit antenna is equipped at the transmitter and one receive antenna is equipped at the receiver. In each time slot, one complex symbol from a Q-level APM constellation $\mathcal{Q}$ is sent from the transmitter to the receiver. Supposing there are T time slots are in each frame. Thus, the frame-wise received signals $\mathbf{y}^{\mathcal{T}} \in \mathbb{C}^{T}$ can be represented as

$$\mathbf{y}^{\mathcal{T}} = \mathbf{h}^{\mathcal{T}} \otimes \mathbf{x}^{\mathcal{T}} + \mathbf{w}^{\mathcal{T}}, \tag{1}$$

where $\mathbf{x}^{\mathcal{T}} \in \mathbb{C}^{T\times 1}$ and $\mathbf{w}^{\mathcal{T}} \in \mathbb{C}^{T\times 1}$ denote the transmitted signals and the complex noise at the receiver. The additive white Gaussian noise (AWGN) is one of the widely adopted noise model. $\mathbf{h}^{\mathcal{T}} \in \mathbb{C}^{L\times 1}$ represents the channel impulse response (CIR) with length L.

In the literature, several time-domain IM schemes have been proposed for the SISO systems to enhance energy efficiency [14], [15]. The principle of the time-domain IM is activating a subset of the time slots in each frame to convey additional information bits on the indices of the activated time slots. Supposing T_{a} time slots are activated in each frame, the transmitted signals will have the following structure

$$\mathbf{x}^{\mathcal{T}} = [\ \underbrace{x_1^{\mathcal{T}}, x_2^{\mathcal{T}}, x_3^{\mathcal{T}}, \cdots, x_T^{\mathcal{T}}}_{T_{\mathrm{a}}\ \text{non-zero elements and}\ (T-T_{\mathrm{a}})\ \text{zeros}}\ ]', \tag{2}$$

where $x_t^{\mathcal{T}}$ $(t = 1, 2, \cdots, T)$ denotes the transmitted symbol at the t-th time slot in a signal frame. Specifically, there are only T_{a} non-zeros elements in each frame and the other $(T - T_{\mathrm{a}})$ elements remain zeros. As a result, $\log_2 \binom{T}{T_{\mathrm{a}}}$ bits can be conveyed by the indices of the activated time slots.

B. MIMO System with Spatial-Domain IM

By deploying more than one antennas at the transmitter and the receiver, a MIMO system is capable of improving the system throughput through spatial multiplying gain, which is widely employed in the current wireless standards [29]. We consider a MIMO system with N transmit antennas and M receive antennas. If the transmitted signals in each time slot are denoted as $\mathbf{x}^{\mathcal{S}} \in \mathbb{C}^{N\times 1}$, the received signals $\mathbf{y}^{\mathcal{S}} \in \mathbb{C}^{M\times 1}$ can be given by

$$\mathbf{y}^{\mathcal{S}} = \mathbf{H}^{\mathcal{S}}\mathbf{x}^{\mathcal{S}} + \mathbf{w}^{\mathcal{S}}, \tag{3}$$

where $\mathbf{w}^{\mathcal{S}} \in \mathbb{C}^{M\times 1}$ represents the complex noise at the receiver. $\mathbf{H}^{\mathcal{S}} \in \mathbb{C}^{M\times N}$ is the channel coefficient matrix, which can be further expressed as

$$\mathbf{H}^{\mathcal{S}} = \begin{bmatrix} h_{1,1}^{\mathcal{S}} & h_{1,2}^{\mathcal{S}} & \cdots & h_{1,N}^{\mathcal{S}} \\ h_{2,1}^{\mathcal{S}} & h_{2,2}^{\mathcal{S}} & \cdots & h_{2,N}^{\mathcal{S}} \\ \vdots & \vdots & h_{m,n}^{\mathcal{S}} & \vdots \\ h_{M,1}^{\mathcal{S}} & h_{M,2}^{\mathcal{S}} & \cdots & h_{M,N}^{\mathcal{S}} \end{bmatrix}, \tag{4}$$

where the element $h_{m,n}^{\mathcal{S}}$ $(m = 1, 2, \cdots, M;\ n = 1, 2, \cdots, N)$ at the m-th row and the n-th column of the matrix stands for the channel coefficient between the n-th transmit antenna and the m-th receive antenna.

When applying spatial-domain IM, not all the transmit antennas are activated at the same time to transmit signals, however, the indices of the activated transmit antennas can be utilized to transmit extra information bits [16]. Supposing N_{a} transmit antennas are activated at each time slot, $\log_2 \binom{N}{N_{\mathrm{a}}}$ bits of information can be transmitted through the indices of the activated antennas according to the principle of spatial-domain IM. Mathematically, the transmitted signals can be expressed as

$$\mathbf{x}^{\mathcal{S}} = [\ \underbrace{x_1^{\mathcal{S}}, x_2^{\mathcal{S}}, x_3^{\mathcal{S}}, \cdots, x_N^{\mathcal{S}}}_{N_{\mathrm{a}}\ \text{non-zero elements and}\ (N-N_{\mathrm{a}})\ \text{zeros}}\ ]', \tag{5}$$

where $x_n^{\mathcal{S}}$ denotes the transmitted signal at the n-th antenna.

C. OFDM System with Frequency-Domain IM

OFDM is a widely used technique for high data rate transmission in modern broadband wireless communication systems [30], such as Wi-Fi and Long-Term Evolution (LTE) systems [31]. Using OFDM, the whole bandwidth is divided into S_{f} subcarriers. The frequency-domain signal $\mathbf{x}^{\mathcal{F}} \in \mathbb{C}^{S_{\mathrm{f}}}$ is generated from a Q-level APM constellation $\mathcal{Q}$. Then it is fed into an S_{f}-point inverse fast Fourier transform (IFFT) module to yield the time-domain signal. After that, the cyclic prefix (CP) is appended to combat the inter symbol interference (ISI).

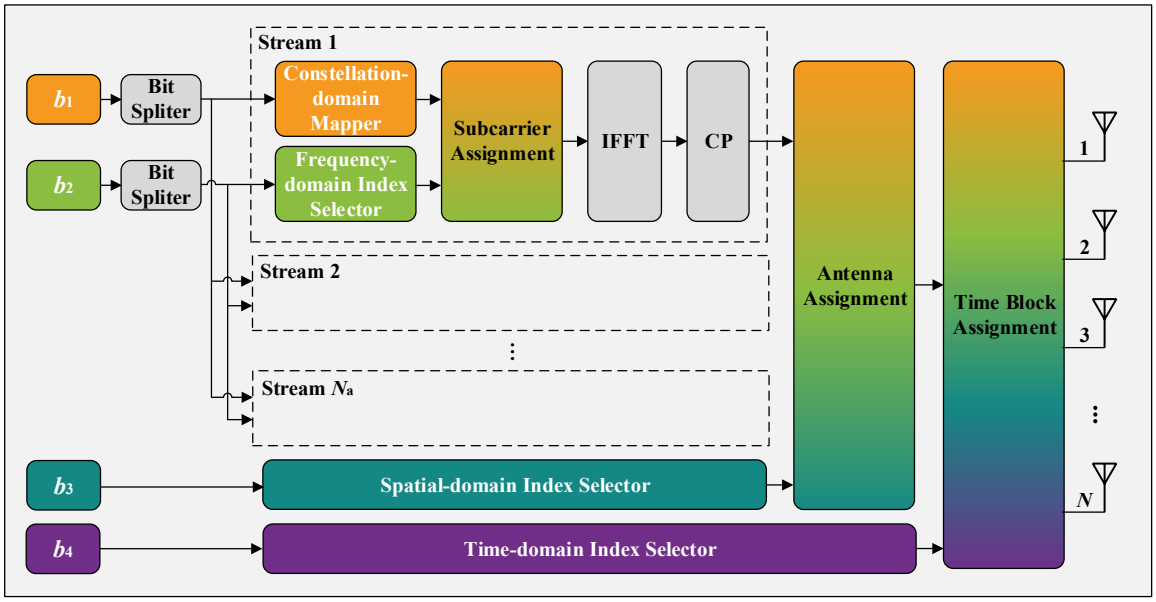


Fig. 2. The block diagram of the transmitter in the proposed IDDMA scheme.

At the receiver, after the removal of CP, the time-domain signal is fed into an S_{f}-point fast Fourier transform (FFT) module to derive the received frequency-domain signal $\mathbf{y}^{\mathcal{F}} \in \mathbb{C}^{S_{\mathrm{f}} \times 1}$, which can be given by

$$\mathbf{y}^{\mathcal{F}} = \mathbf{H}^{\mathcal{F}} \mathbf{x}^{\mathcal{F}} + \mathbf{w}^{\mathcal{F}}, \tag{6}$$

where $\mathbf{w}^{\mathcal{F}} \in \mathbb{C}^{S_{\mathrm{f}} \times 1}$ and $\mathbf{H}^{\mathcal{F}} \in \mathbb{C}^{S_{\mathrm{f}} \times S_{\mathrm{f}}}$ represent the complex noise and the channel coefficient matrix, respectively. When we consider a multi-path channel whose CIR is given by $\mathbf{h}^{\mathcal{F}} \in \mathbb{C}^{L}$, channel matrix $\mathbf{H}^{\mathcal{F}}$ is a diagonal matrix whose diagonal elements are the S_{f}-point FFT of $\mathbf{h}^{\mathcal{F}}$.

Using frequency-domain IM, the subcarriers are split into G groups and each group consists of $S = S_{\mathrm{f}}/G$ subcarriers. In each group, S_{a} out of S subcarriers are activated to transmit information. According to the principle of frequency-domain IM, $\log_2 \binom{S}{S_{\mathrm{a}}}$ information bits are used to select the activated subcarriers and other bits are utilized to decide the Q-level APM constellation symbols at the activated subcarriers [18]. Therefore, the transmitted frequency-domain signals in the g-th subcarrier group $\mathbf{x}_g^{\mathcal{F}}$ $(g = 1, 2, \cdots, G)$ can be expressed as

$$\mathbf{x}_g^{\mathcal{F}} = [\underbrace{x_{(g-1)S+1}^{\mathcal{F}}, x_{(g-1)S+2}^{\mathcal{F}}, x_{(g-1)S+3}^{\mathcal{F}}, \cdots, x_{gS}^{\mathcal{F}}}_{S_{\mathrm{a}} \text{ non-zero elements and } (S-S_{\mathrm{a}}) \text{ zeros}}]', \tag{7}$$

where $x_s^{\mathcal{F}}$ $(s = 1, 2, \cdots, S_{\mathrm{f}})$ denotes the s-th symbol in $\mathbf{x}^{\mathcal{F}}$.

IV. Proposed IDDMA Scheme

Based on the principle of multi-domain IM, the IDDMA scheme is proposed for the multi-user downlink transmission. The designs of the transmitters and receivers are explained in Section IV-A and Section IV-B. In Section IV-C, the special cases are also provided to illustrate the proposed scheme.

A. Transmitter Design

In the proposed IDDMA scheme, the supported users are divided into user clusters. Orthogonal resources are allocated to different user clusters. Specifically, we divide the supported users into clusters of K based on their QoS requirements. In each cluster, only one user is a smart electronic device with high data rate demands and the others are IoT devices with low data rate requirements. The user devices are denoted as U_k $(k = 1, 2, \cdots, K)$, where U_1 represents the smart electronic device and the others are IoT devices. We can conduct the user clustering through many state-of-the-art user clustering methods [32], [33].

In each user cluster, different from the conventional NOMA schemes which utilize power-domain diversities to realize multiple access, the principle of the proposed IDDMA scheme is conveying the information bits for different users on different domains of the transmitted signals, including the constellation domain, the frequency domain, the spatial domain, and the time domain. By doing so, the intra-cluster interference among user devices can be alleviated and the complicated SIC detectors can be avoided at the receivers. Taking the constellation-domain, frequency-domain, spatial-domain, and time-domain manipulation into consideration, we can support up to $K = 4$ users in each user group, which are denoted as U_1, U_2, U_3, and U_4. If we denote the information bits for the four users as $\mathbf{b}_1$, $\mathbf{b}_2$, $\mathbf{b}_3$, and $\mathbf{b}_4$, they are modulated on constellation-domain symbols, frequency-domain symbols, spatial-domain symbols, and time-domain symbols, respectively. Specifically, $\mathbf{b}_1$ is used to decide the constellation-domain symbol from a Q-level APM constellation; $\mathbf{b}_2$ is used to determine the activated subcarriers; $\mathbf{b}_3$ is used to select the activated transmit antennas; and $\mathbf{b}_4$ is used to choose the activated time blocks in a frame.

Mathematically, we consider a multi-user MIMO-OFDM transmitter using multi-domain IM. N transmit antennas are

equipped at the transmitter. The whole bandwidth W is divided into $S_{\rm f}$ subcarriers, which are further grouped into G subcarrier groups with $S = S_{\rm f}/G$ subcarriers in each group. The signals are transmitted in a frame consisting of T time blocks. Due to the principle of multi-domain IM, $N_{\rm a}$ out of N transmit antennas, $S_{\rm a}$ out of S subcarriers in each group, and $T_{\rm a}$ out of T time blocks in each frame are activated to transmit signals.

The block diagram of the proposed IDDMA transmitter is shown in Fig. 2. At the transmitter, the information bits $\mathbf{b}_1$ for U_1 are fed into a bit spliter firstly to derive $(N_{\rm a}GS_{\rm a})$ subsets of bits to decide the constellation-domain symbols on each activated subcarrier in each data stream. $\mathbf{b}_2$ for U_2 is fed into a bit spliter as well to obtain $(N_{\rm a}G)$ subsets to determine the indices of the activated subcarriers in each data stream. We denote the transmitted frequency-domain signals in the v-th $(v = 1, 2, \cdots, N_{\rm a})$ data stream and the g-th $(g = 1, 2, \cdots, G)$ subcarrier group as $\mathbf{x}_g^v \in \mathbb{C}^{S\times 1}$, which can be expressed as

$$\mathbf{x}_g^v = [\underbrace{x^v_{(g-1)S+1},\ x^v_{(g-1)S+2},\ x^v_{(g-1)S+3},\ \cdots,\ x^v_{gS}}_{S_{\rm a}\text{ non}-\text{zero elements and }(S-S_{\rm a})\text{ zeros}}]', \quad (8)$$

where x_s^v denotes the frequency-domain signal in the v-th data stream and the s-th subcarrier. Only $S_{\rm a}$ elements in $\mathbf{x}_g^v$ are non-zero and the other $(S-S_{\rm a})$ elements remain zeros. Therefore, the whole frequency-domain signals in the v-th data stream $\mathbf{x}^v \in \mathbb{C}^{S_{\rm f}\times 1}$ can be derived as

$$\mathbf{x}^v = [\mathbf{x}_1^{v\prime}, \mathbf{x}_2^{v\prime}, \mathbf{x}_3^{v\prime}, \cdots, \mathbf{x}_G^{v\prime}]' = [x_1^v, x_2^v, x_3^v, \cdots, x_{S_{\rm f}}^v]'. \quad (9)$$

Then, the frequency-domain signals are fed into an $S_{\rm f}$-point IFFT module to obtain the time-domain signals. We denote the $S_{\rm f}$-point FFT transformation matrix as $\mathbf{D}$. Therefore, the time-domain signals in the v-th data stream $\dot{\mathbf{x}}^v \in \mathbb{C}^{S_{\rm f}\times 1}$ can be derived as

$$\dot{\mathbf{x}}^v = \mathbf{D}^{\rm H}\mathbf{x}^v. \quad (10)$$

After that, CP is added to the signals to combat ISI, whose length is denoted as $N_{\rm CP}$. We denote the signals with CP in the v-th stream as $\ddot{\mathbf{x}}^v \in \mathbb{C}^{(S_{\rm f}+N_{\rm CP})\times 1}$. Then, the generated $N_{\rm a}$ data stream need to be transmitted through N transmit antennas. The information bits $\mathbf{b}_3$ for user U_3 is utilized to selected $N_{\rm a}$ activated antennas according to the principle of spatial-domain IM. Therefore, the time-domain signals $\ddot{\mathbf{X}} \in \mathbb{C}^{N\times(S_{\rm f}+N_{\rm CP})}$ transmitted from N antennas can be expressed as

$$\begin{aligned}\ddot{\mathbf{X}} &= [\underbrace{\qquad\qquad \ddot{\mathbf{x}}^1, \ddot{\mathbf{x}}^2, \ddot{\mathbf{x}}^3, \cdots, \ddot{\mathbf{x}}^N \qquad\qquad}_{N_{\rm a}\text{ non}-\text{zero elements and }(N-N_{\rm a})\text{ zeros}}]' \\ &= \begin{bmatrix} \ddot{x}_1^1 & \ddot{x}_2^1 & \cdots & \ddot{x}^1_{S_{\rm f}+N_{\rm CP}} \\ \ddot{x}_1^2 & \ddot{x}_2^2 & \cdots & \ddot{x}^2_{S_{\rm f}+N_{\rm CP}} \\ \vdots & \vdots & \ddots & \vdots \\ \ddot{x}_1^N & \ddot{x}_2^N & \cdots & \ddot{x}^N_{S_{\rm f}+N_{\rm CP}} \end{bmatrix},\end{aligned} \quad (11)$$

where each row of $\ddot{\mathbf{X}}$ denotes the transmitted signals from each transmit antenna and each column of $\ddot{\mathbf{X}}$ denotes the transmitted signals at one time slot from N transmit antennas. Due to the principle of spatial-domain IM, only $N_{\rm a}$ rows are non-zero.

In the next step, the information bits $\mathbf{b}_4$ for U_4 is used to choose the activated time blocks in a frame. We add superscripts to $\ddot{\mathbf{X}}$ to denote the signals transmitted in the t-th $(t = 1, 2, \cdots, T)$ time block as $\ddot{\mathbf{X}}^{(t)}$. Due to the principle of time-domain IM, the transmitted signals in each frame $\tilde{\mathbf{X}} \in \mathbb{C}^{N\times T(S_{\rm f}+N_{\rm CP})}$ will have the following structure

$$\tilde{\mathbf{X}} = [\quad \underbrace{\ddot{\mathbf{X}}^{(1)}, \ddot{\mathbf{X}}^{(2)}, \ddot{\mathbf{X}}^{(3)}, \cdots, \ddot{\mathbf{X}}^{(T)}}_{T_{\rm a}\text{ non}-\text{zero elements and }(T-T_{\rm a})\text{ zeros}} \quad]. \quad (12)$$

As a result, only $T_{\rm a}$ elements are non-zero and the other $(T-T_{\rm a})$ elements are zeros.

In the proposed IDDMA scheme, the transmitter should modulate the information bits for different users on the APM symbols and the indices of the activated subcarriers, time slots, and antennas, based on the principle of multi-domain IM. The transmitter can use a look-up table to map the information bits to the indices of the activated subcarriers, time slots, and antennas directly [9]. Therefore, when we use a hash map to store the look-up table, the complexity for selecting the indices of the activated resources will be $\mathcal{O}(1)$. The complexity for choosing the APM symbols on the activated resources will be $\mathcal{O}(GS_aN_aT_a)$. Thus, the total complexity for the transmitter is $\mathcal{O}(GS_aN_aT_a + 1)$. As a result, the proposed IDDMA scheme can decrease the computational complexity at the transmitter and implement flexible multiple access for IoT devices and smart electronic devices. However, a memory is needed to store the look-up tables for the index selection process at the transmitter.

B. Receiver Design

At the receiver side, each user device is equipped with M_k antennas to receive signals. The block diagrams of the receivers for the four users in each user cluster are illustrated in Fig. 3. At each user device, the CPs are first removed to obtain the time-domain signals without CP, which can be given by

$$\dot{\mathbf{Y}}_k^{(t)} = \mathbf{H}_k^{(t)}\dot{\mathbf{X}}^{(t)} + \dot{\mathbf{W}}_k^{(t)}, \quad (13)$$

where $\dot{\mathbf{X}}^{(t)}$ denotes the time-domain signals without CP at the t-th time block. $\ddot{\mathbf{Y}}_k^{(t)} \in \mathbb{C}^{M_k\times S_{\rm f}}$, $\mathbf{H}_k^{(t)} \in \mathbb{C}^{M_k\times N}$, and $\ddot{\mathbf{W}}_k^{(t)} \in \mathbb{C}^{M_k\times S_{\rm f}}$ denote the received time-domain signals, the Rayleigh flat fading channel, and the AWGN noise at the t-th time block for the k-th user.

In the proposed IDDMA scheme, since the information bits for the four users in each user cluster are conveyed by different domains of the transmitted signals, the users U_1, U_2, U_3, and U_4 are required to demodulate the constellation-, frequency-, spatial-, and time-domain signals, respectively. The maximum likelihood (ML) detectors can be used to achieve optimal detection performance. However, the exhaust search applied in ML detectors involves intractable computational complexity, which cannot be tolerated by the IoT devices U_2, U_3, and U_4. Therefore, we propose a low-complexity detection method for the IoT users based on the maximum ratio combination (MRC) algorithms [34] in order to avoid the use of SIC and reduce detection complexity.

For user U_4, the activated time blocks need to be detected. We denote the estimated time-domain symbols as $\hat{\mathbf{z}}_4$, which

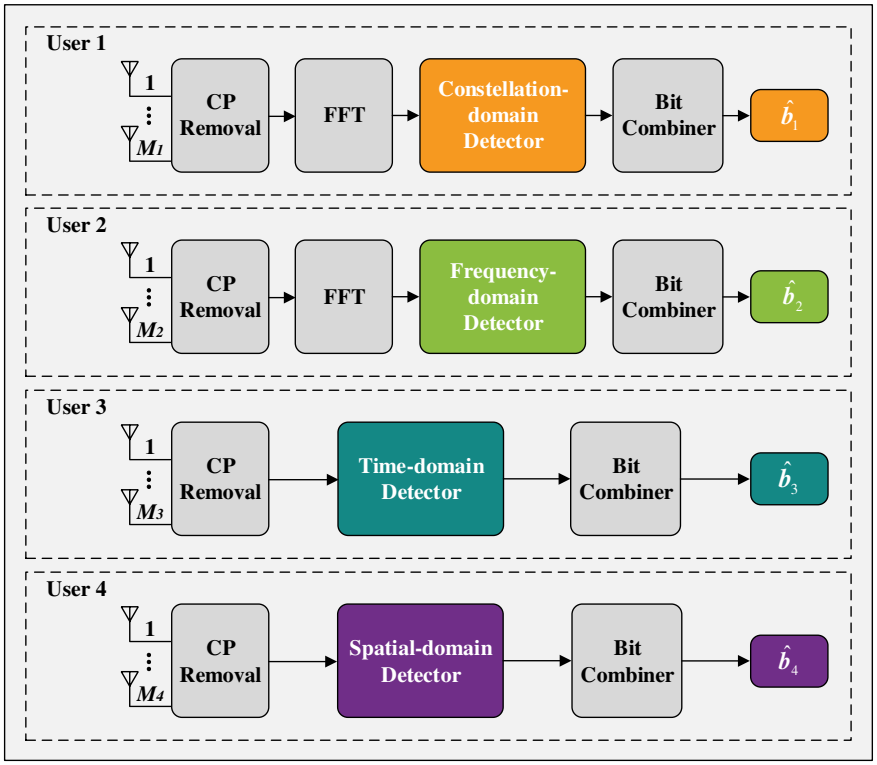


Fig. 3. The block diagrams of the receivers in the proposed IDDMA scheme.

can be derived by selecting T_{a} time blocks with the largest Frobenius norm, which can be expressed as

$$\hat{\mathbf{z}}_4 = \arg \max_{t_1,t_2,\cdots,t_{T_{\mathrm{a}}}} \left(\sum_{j=1}^{T_{\mathrm{a}}} \|\dot{\mathbf{Y}}_4^{(t_j)}\|_{\mathrm{F}}^2 \right). \tag{14}$$

Then, the estimated $\hat{\mathbf{z}}_4$ can be utilized to decode the information bits $\hat{\mathbf{b}}_4$.

For user U_3, a equalizer is applied firstly to equalize the channel fading. The linear equalizers including zero forcing (ZF) equalizer and minimum mean square error (MMSE) equalizer can be adopted to reduce detection complexity. When using ZF equalizer, the estimated time-domain signals can be derived as

$$\hat{\dot{\mathbf{X}}}^{(t)} = {\mathbf{H}_3^{(t)}}^{\dagger} \dot{\mathbf{Y}}_3^{(t)} = {\mathbf{H}_3^{(t)}}^{\dagger} \mathbf{H}_3^{(t)} \dot{\mathbf{X}}^{(t)} + {\mathbf{H}_3^{(t)}}^{\dagger} \dot{\mathbf{W}}_3^{(t)}. \tag{15}$$

We denote the estimated spatial-domain symbols for U_3 as $\hat{\mathbf{z}}_3$. Then, U_3 selects N_{a} rows of $\hat{\dot{\mathbf{X}}}_t$ with the largest Frobenius norm as the estimated activated transmit antennas, which can be given by

$$\hat{\mathbf{z}}_3 = \arg \max_{i_1,i_2,\cdots,i_{N_{\mathrm{a}}}} \left(\sum_{v=1}^{N_{\mathrm{a}}} \|\hat{\dot{\mathbf{X}}}_{(i_v,\ :)}^{(t)}\|_{\mathrm{F}}^2 \right), \tag{16}$$

where $\hat{\dot{\mathbf{X}}}_{(i_v,\ :)}^{(t)}$ denotes the i_v-th row of $\hat{\dot{\mathbf{X}}}^{(t)}$. After that, the estimated $\hat{\mathbf{z}}_3$ is used to decode the bit information $\hat{\mathbf{b}}_3$ for U_3. Here a threshold η_3 is involved to prevent U_3 from decoding zero time blocks caused by time-domain IM. The estimated $\hat{\mathbf{z}}_3$ will be decoded if $\|\hat{\dot{\mathbf{X}}}_{(\hat{\mathbf{z}}_3,\ :)}^{(t)}\|_{\mathrm{F}}^2 > \eta_3$, otherwise, it will not.

For user U_2, after CP removal, the time-domain signals are fed into an FFT module to derive the frequency-domain signals $\hat{\mathbf{Y}}_2^{(t)} \in \mathbb{C}^{M_k \times S_{\mathrm{f}}}$, which can be expressed as

$$\hat{\mathbf{Y}}_2^{(t)} = \dot{\mathbf{Y}}_2^{(t)} \mathbf{D}' = \mathbf{H}_2^{(t)} \dot{\mathbf{X}}^{(t)} \mathbf{D}' + \dot{\mathbf{W}}_2^{(t)} \mathbf{D}' = \mathbf{H}_2^{(t)} \mathbf{X}^{(t)} + \mathbf{W}_2^{(t)}, \tag{17}$$

where $\mathbf{X}^{(t)} = \dot{\mathbf{X}}^{(t)} \mathbf{D}'$ and $\mathbf{W}_2^{(t)} = \dot{\mathbf{W}}_2^{(t)} \mathbf{D}'$ denote the frequency-domain signals and noise, respectively. Then, a equalizer is applied to obtain the estimation of the transmitted frequency-domain signals. When using ZF equalizer, the frequency-domain signals can be derived as

$$\hat{\mathbf{X}}^{(t)} = {\mathbf{H}_2^{(t)}}^{\dagger} \hat{\mathbf{Y}}_2^{(t)} = {\mathbf{H}_2^{(t)}}^{\dagger} \mathbf{H}_2^{(t)} \mathbf{X}^{(t)} + {\mathbf{H}_2^{(t)}}^{\dagger} \mathbf{W}_2^{(t)}, \tag{18}$$

where each row of $\hat{\mathbf{X}}^{(t)}$ represents the transmitted frequency-domain signals from a specific transmit antenna. Recall that the information for U_2 is conveyed by the indices of the activated subcarriers in each subcarrier group. We denote the n-th row of $\hat{\mathbf{X}}^{(t)}$ as $\hat{\mathbf{x}}^{(t,n)} = [\hat{x}_1^{(t,n)}, \hat{x}_2^{(t,n)}, \cdots, \hat{x}_{S_{\mathrm{f}}}^{(t,n)}]$. Therefore, the estimated frequency-domain symbols for the g-th subcarrier group can be derived by selecting S_{a} elements with the largest absolute value, which can be given by

$$\hat{\mathbf{z}}_2^{(g,n)} = \arg \max_{l_1,l_2,\cdots,l_{S_{\mathrm{a}}}} \left(\sum_{s=1}^{S_{\mathrm{a}}} \|\hat{x}_{(g-1)S+l_s}^{(t,n)}\|_{\mathrm{F}}^2 \right). \tag{19}$$

Then, the estimated $\hat{\mathbf{z}}_2^{(g,n)}$ is used to decode the bit information $\hat{\mathbf{b}}_2$ for U_2. Similar to U_3, a threshold η_2 is also involved to prevent U_2 from decoding zero frequency-domain signals from the inactive antennas caused by spatial-domain IM.

For user U_1, which is a smart electronic device with

sufficient computing resources. The ML detection method can be employed to achieve the optimal detection performance by exhaust search in all possible constellation-domain symbols. The estimated constellation-domain symbols $\hat{\mathbf{z}}_1$ can be given by

$$\hat{\mathbf{z}}_1 = \arg \max_{j_1, j_2, \cdots, j_{NS_\mathrm{f}} \in \{0, \mathcal{Q}\}} \left(\| \dot{\mathbf{Y}}_1^{(t)} - \mathbf{H}_1^{(t)} \dot{\mathbf{X}}^{(t)}[j_1, j_2, \cdots, j_{NS_\mathrm{f}}] \|_\mathrm{F}^2 \right) \tag{20}$$

where $j_1, j_2, \cdots, j_{NS_\mathrm{f}}$ denote NS_f constellation-domain symbols conveyed by $\dot{\mathbf{X}}^{(t)}$. The specific transmitted signals determined by $j_1, j_2, \cdots, j_{NS_\mathrm{f}}$ are denoted as $\dot{\mathbf{X}}^{(t)}[j_1, j_2, \cdots, j_{NS_\mathrm{f}}]$. Then, the estimated information bits $\hat{\mathbf{b}}_1$ can be derived from $\hat{\mathbf{z}}_1$. The MRC-based detection method can also be employed to decrease detection complexity, which consists of two steps. In the two-step method, the indices of the activated resources are firstly decoded similar to U_2, U_3, and U_4. Then, the APM symbols on the activated resources are further decoded to get the information bits $\hat{\mathbf{b}}_1$.

In practical communication systems, the detection mechanism of the IoT devices can be either pre-designed or flexibly chosen, which should be selected based on the computational capacities of the IoT devices. On the one hand, when the IoT devices only have limited computational capacities, they are encouraged to use the pre-designed mechanism, where each device is equipped with one detector for specific domain signals. The system should carefully group the users detecting different domains in one user cluster, and divide the users detecting the same domain in different user clusters. Corresponding user grouping algorithms should be developed and conducted at the transmitter. On the other hand, when the IoT devices have enough computational capacities, the IoT devices can be equipped with multiple detectors for different domains and flexibly choose the domains. The time domain can be used as the default option, and specific signals can be used to indicate the right domain for the IoT devices in their initialization phase to decrease the complexity at the IoT devices.

C. Special Cases

Under the proposed IDDMA framework, the transmission mechanism can be flexibly adjusted according to the requirements of the communication systems, which induces several special cases of the proposed scheme. These special cases are important components of the IDDMA framework and can be easily employed in the current and future wireless communication systems.

We can employ less domains of IM techniques for simplified systems. For instance, we can employ the IM technique in only one domain to facilitate multiple access services for two users in each user cluster, i.e., a smart electronic device and an IoT device. The information bits for the smart electronic device is modulated on constellation-domain APM symbols, and the information bits for the IoT device can be modulated on time-domain symbols, spatial-domain symbols, or frequency-domain symbols, when employing the time-domain IM, spatial-domain IM, or frequency-domain IM, respectively. We denote these cases as time-domain IDDMA (TD-IDDMA), spatial-domain IDDMA (SD-IDDMA), and frequency-domain IDDMA (FD-IDDMA), accordingly, the block diagrams of which are illustrated in Fig. 4(a), Fig. 4(b), and Fig. 4(c), respectively. At the receiver side, the smart electronic device needs to demodulate the APM symbols, and the IoT devices only need to decode the indices of the activated antennas, subcarriers, or time slots, respectively. Due to the principle of the proposed method, the information bits for the two users in each cluster are modulated on different domains of the signals. As a result, the intra-cluster interference is alleviated and the SIC detectors are also avoided at the receivers, which is friendly to the IoT devices with limited computing capacities.

We can also employ two domains of IM techniques in the communication system to facilitate three users in each user cluster. For example, when employing both frequency- and spatial-domain IM in a MIMO-OFDM communication system, we can support one smart electronic device and two IoT devices in each user cluster. The information bits for the smart electronic device and the two IoT devices can be modulated on the APM constellation, the indices of the activated subcarriers, and the indices of the activated antennas, respectively. Similarly, no SIC detector is needed at the receiver side to manage the interference of other users in the same user cluster.

According to [4], the key requirements of IoT applications include massive connection, extended coverage, low device cost, and low power operation. The proposed scheme is able to support several IoT devices in the same spectrum bands with smart electronic devices. Therefore, it can support both the IoT applications and mobile broadband applications within a single network. This will further enhance the number of connections for IoT applications and will be a key enabler for the future massive connections of IoT applications according to [4]. Using the proposed scheme, the areas already covered by mobile broadband network can also support IoT applications easily, which will extend the coverage area of IoT applications. Moreover, the proposed scheme is able to reduce the computational complexity at the IoT devices. Thus, low-power processor can be installed at the IoT devices to reduce the power consumption of IoT devices.

V. Performance Analysis

In this section, we analyze the performance of the proposed IDDMA scheme. In Section V-A, we analyze the achievable rate of the proposed schemes through mutual information calculation. Closed form lower bounds of the achievable rates are derived and closed form approximations are further obtained to provide efficient estimation of the achievable rate for the special cases of the proposed scheme. Then, the computational complexity at the receiver is evaluated as well in Section V-B.

A. Achievable Rate Analyses

We denote the constellation-domain, frequency-domain, spatial-domain, and time-domain symbols as $\mathcal{X}^\mathcal{C}$, $\mathcal{X}^\mathcal{F}$, $\mathcal{X}^\mathcal{S}$, and $\mathcal{X}^\mathcal{T}$, respectively. In the following paragraphs, we derive the lower bounds and approximations of the achievable rates for the special cases SD-IDDMA, FD-IDDMA, and TD-IDDMA, respectively. The lower bound of the achievable sum rate using SD-IDDMA can be given in *Proposition 1*.

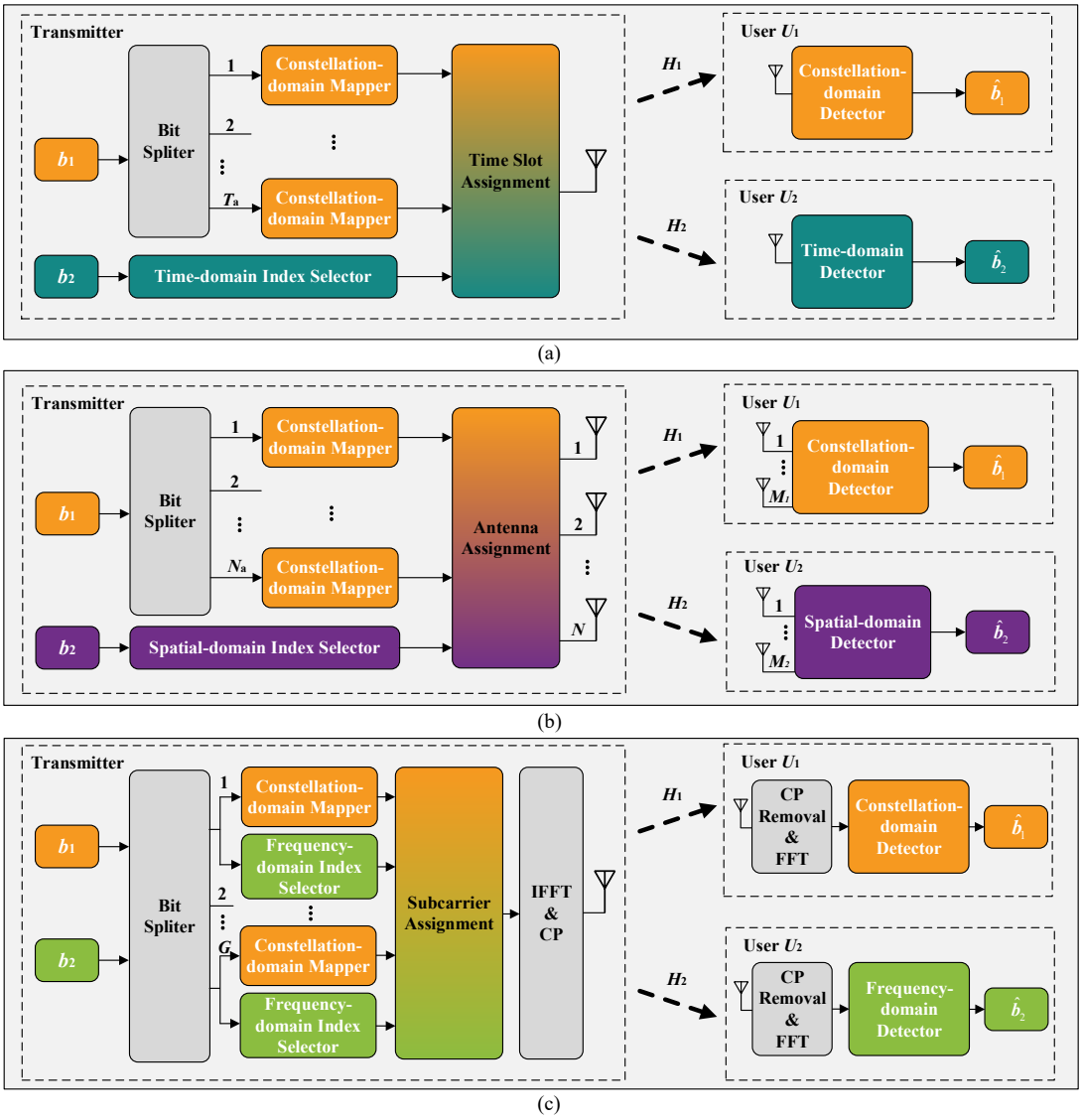


Fig. 4. The block diagram of the special cases of the proposed IDDMA scheme: a) the TD-IDDMA scheme; b) the SD-IDDMA scheme; c) the FD-IDDMA scheme.

Proposition 1: For a multi-user MIMO communication system defined in Section III-B with N transmit antennas at the base station, M_1 and M_2 receive antennas at users U_1 and U_2, where the proposed SD-IDDMA is adopted with $N_{\rm a}$ active antennas, the achievable sum rate for the two users in each user cluster can be lower bounded by

$$R^{\mathcal{S}} \geq \frac{W}{\binom{N}{N_{\rm a}}} \sum_{p=1}^{\binom{N}{N_{\rm a}}} \sum_{q\in\Psi_p} \log_2\left(1+\frac{\sigma_{p,q}^2 P}{N_{\rm a} N_0 W}\right) + W\log_2\left(\frac{\binom{N}{N_{\rm a}}}{e^{M_2}}\right) - \frac{W}{\binom{N}{N_{\rm a}}} \sum_{p=1}^{\binom{N}{N_{\rm a}}} \log_2\left(\sum_{r=1}^{\binom{N}{N_{\rm a}}} \frac{|\Sigma_p^{\mathcal{S}}|}{|\Sigma_p^{\mathcal{S}}+\Sigma_r^{\mathcal{S}}|}\right), \tag{21}$$

where W, P, N_0, and Ψ_p denote the bandwidth, the total transmit power of the signals, the power density of the AWGN, and the index set of the p-th spatial-domain symbol, respectively.

Proof: According to the system model in Section III-B, the received signals by the two users U_k $(k=1,2)$ can be given by

$$\mathbf{y}_k^{\mathcal{S}} = \mathbf{H}_k^{\mathcal{S}}\mathbf{x}^{\mathcal{S}} + \mathbf{w}_k^{\mathcal{S}}. \tag{22}$$

Because of the chain rule of the mutual information, we have

$$\begin{aligned}\mathcal{I}(\mathbf{x}^{\mathcal{S}};\mathbf{y}_k^{\mathcal{S}}) &= \mathcal{I}(\mathcal{X}^{\mathcal{C}},\mathcal{X}^{\mathcal{S}};\mathbf{y}_k^{\mathcal{S}}) \\ &= \mathcal{I}(\mathcal{X}^{\mathcal{C}};\mathbf{y}_k^{\mathcal{S}}|\mathcal{X}^{\mathcal{S}}) + \mathcal{I}(\mathcal{X}^{\mathcal{S}};\mathbf{y}_k^{\mathcal{S}}).\end{aligned} \tag{23}$$

Thus, the mutual information for the users can be divided into two parts, the spatial-domain mutual information $\mathcal{I}(\mathcal{X}^{\mathcal{S}};\mathbf{y}_k^{\mathcal{S}})$ and the constellation-domain mutual information $\mathcal{I}(\mathcal{X}^{\mathcal{C}};\mathbf{y}_k^{\mathcal{S}}|\mathcal{X}^{\mathcal{S}})$.

In the proposed scheme, only the constellation-domain information is intended for the first user U_1. We assume the channel state information (CSI) is unknown at the transmitter, and the transmit power is allocated to each antenna equally.

According to [35], on the condition that the spatial-domain symbol is chosen, the constellation-domain mutual information can be given by

$$\mathcal{I}(\mathcal{X}^{\mathcal{C}};\mathbf{y}_1^{\mathcal{S}}|\mathcal{X}^{\mathcal{S}}=\Psi_p)=\sum_{q\in\Psi_p}\log_2\left(1+\frac{\sigma_{p,q}^2P}{N_{\mathrm{a}}N_0W}\right), \quad (24)$$

where $\sigma_{p,q}$ represents the q-th singular value of the sub-channel matrix for the spatial-domain symbol Ψ_p. Supposing the input bits are selected arbitrarily, the spatial-domain symbols are selected with equal probability. Therefore, the mutual information for U_1 can be expressed as

$$\begin{aligned}\mathcal{I}(\mathcal{X}^{\mathcal{C}};\mathbf{y}_1^{\mathcal{S}}|\mathcal{X}^{\mathcal{S}})&=\sum_{p=1}^{\binom{N}{N_{\mathrm{a}}}}\Pr(\mathcal{X}^{\mathcal{S}}=\Psi_p)\times\mathcal{I}(\mathcal{X}^{\mathcal{C}};\mathbf{y}_1^{\mathcal{S}}|\mathcal{X}^{\mathcal{S}}=\Psi_p)\\&=\frac{1}{\binom{N}{N_{\mathrm{a}}}}\sum_{p=1}^{\binom{N}{N_{\mathrm{a}}}}\sum_{q\in\Psi_p}\log_2\left(1+\frac{\sigma_{p,q}^2P}{N_{\mathrm{a}}N_0W}\right).\end{aligned} \quad (25)$$

As a result, the achievable rate for the first user U_1 can be expressed as

$$R_1^{\mathcal{S}}=W\times\mathcal{I}(\mathcal{X}^{\mathcal{C}};\mathbf{y}_1^{\mathcal{S}}|\mathcal{X}^{\mathcal{S}})=\frac{W}{\binom{N}{N_{\mathrm{a}}}}\sum_{p=1}^{\binom{N}{N_{\mathrm{a}}}}\sum_{q\in\Psi_p}\log_2\left(1+\frac{\sigma_{p,q}^2P}{N_{\mathrm{a}}N_0W}\right). \quad (26)$$

On the other hand, only the spatial-domain information is intended for the second user U_2. The spatial-domain mutual information can be expressed as

$$\begin{aligned}\mathcal{I}(\mathcal{X}^{\mathcal{S}};\mathbf{y}_2^{\mathcal{S}})=&\sum_{p=1}^{\binom{N}{N_{\mathrm{a}}}}\Pr(\mathcal{X}^{\mathcal{S}}=\Psi_p)\times\int_{\mathbf{y}_2^{\mathcal{S}}}f(\mathbf{y}_2^{\mathcal{S}}|\mathcal{X}^{\mathcal{S}}=\Psi_p)\times\\&\log_2\left(\frac{f(\mathbf{y}_2^{\mathcal{S}}|\mathcal{X}^{\mathcal{S}}=\Psi_p)}{f(\mathbf{y}_2^{\mathcal{S}})}\right)\mathrm{d}\mathbf{y}_2^{\mathcal{S}}\\=&\frac{1}{\binom{N}{N_{\mathrm{a}}}}\sum_{p=1}^{\binom{N}{N_{\mathrm{a}}}}\int_{\mathbf{y}_2^{\mathcal{S}}}f(\mathbf{y}_2^{\mathcal{S}}|\mathcal{X}^{\mathcal{S}}=\Psi_p)\times\\&\log_2\left(\frac{f(\mathbf{y}_2^{\mathcal{S}}|\mathcal{X}^{\mathcal{S}}=\Psi_p)}{f(\mathbf{y}_2^{\mathcal{S}})}\right)\mathrm{d}\mathbf{y}_2^{\mathcal{S}},\end{aligned} \quad (27)$$

where $f(\mathbf{y}_2^{\mathcal{S}})$ and $f(\mathbf{y}_2^{\mathcal{S}}|\mathcal{X}^{\mathcal{S}}=\Psi_p)$ represent the probability density function (PDF) of $\mathbf{y}_2^{\mathcal{S}}$ and the conditional PDF of $\mathbf{y}_2^{\mathcal{S}}$, respectively. According to the total probability theorem, the PDF of $\mathbf{y}_2^{\mathcal{S}}$ can be given by

$$f(\mathbf{y}_2^{\mathcal{S}})=\frac{1}{\binom{N}{N_{\mathrm{a}}}}\sum_{p=1}^{\binom{N}{N_{\mathrm{a}}}}f(\mathbf{y}_2^{\mathcal{S}}|\mathcal{X}^{\mathcal{S}}=\Psi_p). \quad (28)$$

And the conditional PDF can be further given by

$$f(\mathbf{y}_2^{\mathcal{S}}|\mathcal{X}^{\mathcal{S}}=\Psi_p)=\frac{1}{\pi^{M_2}|\Sigma_p^{\mathcal{S}}|}\exp\left(-\mathbf{y}_2^{\mathcal{S}\mathrm{H}}{\Sigma_p^{\mathcal{S}}}^{-1}\mathbf{y}_2^{\mathcal{S}}\right), \quad (29)$$

where $\Sigma_p^{\mathcal{S}}$ represents the covariance matrix of $\mathbf{y}_2^{\mathcal{S}}$ when the spatial-domain symbol is $\mathcal{X}^{\mathcal{S}}=\Psi_p$. The mutual information in (27) has no closed-form expression. We further divide it into two parts

$$I(\mathcal{X}^{\mathcal{S}};\mathbf{y}_2^{\mathcal{S}})=\frac{1}{\binom{N}{N_{\mathrm{a}}}}\sum_{p=1}^{\binom{N}{N_{\mathrm{a}}}}(\Gamma_{p,1}-\Gamma_{p,2}). \quad (30)$$

The first part can be calculated as

$$\begin{aligned}\Gamma_{p,1}&\triangleq\int_{\mathbf{y}_2^{\mathcal{S}}}f(\mathbf{y}_2^{\mathcal{S}}|\mathcal{X}^{\mathcal{S}}=\Psi_p)\times\log_2\left(f(\mathbf{y}_2^{\mathcal{S}}|\mathcal{X}^{\mathcal{S}}=\Psi_p)\right)\mathrm{d}\mathbf{y}_2^{\mathcal{S}}\\&=-M_2\log_2(\pi e)-\log_2\left(|\Sigma_p^{\mathcal{S}}|\right),\end{aligned} \quad (31)$$

and the second part can be expressed as

$$\Gamma_{p,2}\triangleq\int_{\mathbf{y}_2^{\mathcal{S}}}f(\mathbf{y}_2^{\mathcal{S}}|\mathcal{X}^{\mathcal{S}}=\Psi_p)\times\log_2\left(\frac{1}{\binom{N}{N_{\mathrm{a}}}}\sum_{r=1}^{\binom{N}{N_{\mathrm{a}}}}f(\mathbf{y}_2^{\mathcal{S}}|\mathcal{X}^{\mathcal{S}}=\Psi_r)\right)\mathrm{d}\mathbf{y}_2^{\mathcal{S}}. \quad (32)$$

Due to the concavity of the $\log_2(\cdot)$ function, the Jensen's inequality can be utilized to derive the upper bound of (32), which can be expressed as

$$\begin{aligned}\Gamma_{p,2}&\le\log_2\left(\frac{1}{\binom{N}{N_{\mathrm{a}}}}\sum_{r=1}^{\binom{N}{N_{\mathrm{a}}}}\int_{\mathbf{y}_2^{\mathcal{S}}}f(\mathbf{y}_2^{\mathcal{S}}|\mathcal{X}^{\mathcal{S}}=\Psi_p)\times f(\mathbf{y}_2^{\mathcal{S}}|\mathcal{X}^{\mathcal{S}}=\Psi_r)\mathrm{d}\mathbf{y}_2^{\mathcal{S}}\right)\\&=-M_2\log_2(\pi)+\log_2\left(\frac{1}{\binom{N}{N_{\mathrm{a}}}}\sum_{r=1}^{\binom{N}{N_{\mathrm{a}}}}\frac{1}{|\Sigma_p^{\mathcal{S}}+\Sigma_r^{\mathcal{S}}|}\right).\end{aligned} \quad (33)$$

Therefore, the lower bound of the mutual information for the second user is yielded as

$$I(\mathcal{X}^{\mathcal{S}};\mathbf{y}_2^{\mathcal{S}})\ge\log_2\left(\frac{\binom{N}{N_{\mathrm{a}}}}{e^{M_2}}\right)-\frac{1}{\binom{N}{N_{\mathrm{a}}}}\sum_{p=1}^{\binom{N}{N_{\mathrm{a}}}}\log_2\left(\sum_{r=1}^{\binom{N}{N_{\mathrm{a}}}}\frac{|\Sigma_p^{\mathcal{S}}|}{|\Sigma_p^{\mathcal{S}}+\Sigma_r^{\mathcal{S}}|}\right). \quad (34)$$

As a result, the lower bound of the achievable rate of the second user U_2 is expressed as

$$\begin{aligned}R_2^{\mathcal{S}}&=W\times\mathcal{I}(\mathcal{X}^{\mathcal{S}};\mathbf{y}_2^{\mathcal{S}})\\&\ge W\log_2\left(\frac{\binom{N}{N_{\mathrm{a}}}}{e^{M_2}}\right)-\frac{W}{\binom{N}{N_{\mathrm{a}}}}\sum_{p=1}^{\binom{N}{N_{\mathrm{a}}}}\log_2\left(\sum_{r=1}^{\binom{N}{N_{\mathrm{a}}}}\frac{|\Sigma_p^{\mathcal{S}}|}{|\Sigma_p^{\mathcal{S}}+\Sigma_r^{\mathcal{S}}|}\right).\end{aligned} \quad (35)$$

Finally, the lower bound of the achievable sum rate can be derived as

$$\begin{aligned}R^{\mathcal{S}}=&R_1^{\mathcal{S}}+R_2^{\mathcal{S}}\\\ge&\frac{W}{\binom{N}{N_{\mathrm{a}}}}\sum_{p=1}^{\binom{N}{N_{\mathrm{a}}}}\sum_{q\in\Psi_p}\log_2\left(1+\frac{\sigma_{p,q}^2P}{N_{\mathrm{a}}N_0W}\right)+W\log_2\left(\frac{\binom{N}{N_{\mathrm{a}}}}{e^{M_2}}\right)\\&-\frac{W}{\binom{N}{N_{\mathrm{a}}}}\sum_{p=1}^{\binom{N}{N_{\mathrm{a}}}}\log_2\left(\sum_{r=1}^{\binom{N}{N_{\mathrm{a}}}}\frac{|\Sigma_p^{\mathcal{S}}|}{|\Sigma_p^{\mathcal{S}}+\Sigma_r^{\mathcal{S}}|}\right).\end{aligned} \quad (36)$$

■

An approximation of the achievable sum rate can be further obtained in *Corollary 1* to provide efficient estimation of the achievable sum rate for the SD-IDDMA scheme.

Corollary 1: In the SD-IDDMA scheme, the achievable sum rate of the two users in one user cluster can be approximated as

$$R^{\mathcal{S}} \approx \frac{W}{\binom{N}{N_{\mathrm{a}}}} \sum_{p=1}^{\binom{N}{N_{\mathrm{a}}}} \sum_{q\in\Psi_p} \log_2\left(1+\frac{\sigma_{p,q}^2 P}{N_{\mathrm{a}} N_0 W}\right) + W\log_2\left(\frac{\binom{N}{N_{\mathrm{a}}}}{2^{M_2}}\right) - \frac{W}{\binom{N}{N_{\mathrm{a}}}} \sum_{p=1}^{\binom{N}{N_{\mathrm{a}}}} \log_2\left(\sum_{r=1}^{\binom{N}{N_{\mathrm{a}}}} \frac{|\Sigma_p^{\mathcal{S}}|}{|\Sigma_p^{\mathcal{S}}+\Sigma_r^{\mathcal{S}}|}\right). \tag{37}$$

Proof: It can be calculated that the lower bound of the achievable rate of U_2 in (35) approaches $-M_2 W\log_2(e/2)$ and $W\log_2\left(\binom{N}{N_{\mathrm{a}}}\right) - M_2 W\log_2(e/2)$ in the low and high signal to noise ratio (SNR) regions. There exists a gap of $M_2 W\log_2(e/2)$ between the lower bound and the true value in the low and high SNR regions, since the true value is supposed to be 0 and $W\log_2\left(\binom{N}{N_{\mathrm{a}}}\right)$. Thus, we apply a constant shift of $M_2 W\log_2(e/2)$ to the lower bound to derive an approximation, which is

$$R_2^{\mathcal{S}} \approx W\log_2\left(\frac{\binom{N}{N_{\mathrm{a}}}}{2^{M_2}}\right) - \frac{W}{\binom{N}{N_{\mathrm{a}}}} \sum_{p=1}^{\binom{N}{N_{\mathrm{a}}}} \log_2\left(\sum_{r=1}^{\binom{N}{N_{\mathrm{a}}}} \frac{|\Sigma_p^{\mathcal{S}}|}{|\Sigma_p^{\mathcal{S}}+\Sigma_r^{\mathcal{S}}|}\right). \tag{38}$$

Thus, the result (37) can be derived by substituting (26) and (38) into $R^{\mathcal{S}} = R_1^{\mathcal{S}} + R_2^{\mathcal{S}}$. ∎

Then, we analyze the achievable rate of the FD-IDDMA scheme, where the frequency-selective channel is considered. The lower bound of the achievable sum rate can be derived in *Proposition 2*.

Proposition 2: For a multi-user OFDM communication system defined in Section III-C with S_{f} subcarriers divided into G groups, where the proposed FD-IDDMA is adopted with S_{a} out of S subcarriers are activated in each subcarrier group, the achievable sum rate for the two users in each user cluster can be lower bounded by

$$R^{\mathcal{F}} \geq \frac{W S_{\mathrm{a}} S_{\mathrm{f}}}{S^2(S_{\mathrm{f}}+N_{\mathrm{CP}})} \sum_{q=1}^{S} \log_2\left(1+\frac{{H_{1,q}^{\mathcal{F}}}^2 PS}{S_{\mathrm{a}} N_0 W}\right) + \frac{W S_{\mathrm{f}}}{S(S_{\mathrm{f}}+N_{\mathrm{CP}})} \times \log_2\left(\frac{\binom{S}{S_{\mathrm{a}}}}{e^S}\right) - \frac{W S_{\mathrm{f}}}{S(S_{\mathrm{f}}+N_{\mathrm{CP}})\binom{S}{S_{\mathrm{a}}}} \sum_{p=1}^{\binom{S}{S_{\mathrm{a}}}} \log_2\left(\sum_{r=1}^{\binom{S}{S_{\mathrm{a}}}} \frac{|\Sigma_p^{\mathcal{F}}|}{|\Sigma_p^{\mathcal{F}}+\Sigma_r^{\mathcal{F}}|}\right), \tag{39}$$

where W, P, N_0, and N_{CP} denote the bandwidth, the total transmit power, the power density of the AWGN, and the length of CP, respectively.

Proof: The received signals by the two users U_k $(k = 1, 2)$ can be given by

$$\mathbf{y}_k^{\mathcal{F}} = \mathbf{H}_k^{\mathcal{F}} \mathbf{x}^{\mathcal{F}} + \mathbf{w}_k^{\mathcal{F}}. \tag{40}$$

Due to the chain rule of mutual information, the total mutual information for the k-th user is given by

$$\mathcal{I}(\mathbf{x}^{\mathcal{F}}; \mathbf{y}_k^{\mathcal{F}}) = \mathcal{I}(\mathcal{X}^{\mathcal{C}}, \mathcal{X}^{\mathcal{F}}; \mathbf{y}_k^{\mathcal{F}}) = \mathcal{I}(\mathcal{X}^{\mathcal{C}}; \mathbf{y}_k^{\mathcal{F}}|\mathcal{X}^{\mathcal{F}}) + \mathcal{I}(\mathcal{X}^{\mathcal{F}}; \mathbf{y}_k^{\mathcal{F}}), \tag{41}$$

where $\mathcal{I}(\mathcal{X}^{\mathcal{C}}; \mathbf{y}_k^{\mathcal{F}}|\mathcal{X}^{\mathcal{F}})$ and $\mathcal{I}(\mathcal{X}^{\mathcal{F}}; \mathbf{y}_k^{\mathcal{F}})$ represent the mutual information conveyed by the constellation-domain and frequency-domain symbols, respectively. For the first user, the mutual information conveyed by the constellation-domain symbols can be given by

$$\mathcal{I}(\mathcal{X}^{\mathcal{C}}; \mathbf{y}_1^{\mathcal{F}}|\mathcal{X}^{\mathcal{F}}) = \sum_{p=1}^{\binom{S}{S_{\mathrm{a}}}} \Pr(\mathcal{X}^{\mathcal{F}} = \Phi_p) \times \mathcal{I}(\mathcal{X}^{\mathcal{C}}; \mathbf{y}_1^{\mathcal{F}}|\mathcal{X}^{\mathcal{F}} = \Phi_p), \tag{42}$$

where Φ_p denotes the index set of the p-th frequency-domain symbol. Supposing the index-domain symbols are selected with equal probability and the power is allocated equally for each subcarrier, the mutual information under Gaussian inputs for the first user can be further given by

$$\begin{aligned}\mathcal{I}(\mathcal{X}^{\mathcal{C}}; \mathbf{y}_1^{\mathcal{F}}|\mathcal{X}^{\mathcal{F}}) &= \frac{1}{\binom{S}{S_{\mathrm{a}}}} \sum_{p=1}^{\binom{S}{S_{\mathrm{a}}}} \sum_{q\in\Phi_p} \log_2\left(1+\frac{{H_{1,q}^{\mathcal{F}}}^2 P/GS_{\mathrm{a}}}{N_0 W/GS}\right) \\ &= \frac{S_{\mathrm{a}}}{S} \sum_{q=1}^{S} \log_2\left(1+\frac{{H_{1,q}^{\mathcal{F}}}^2 PS}{S_{\mathrm{a}} N_0 W}\right),\end{aligned} \tag{43}$$

where $H_{1,q}^{\mathcal{F}}$ denotes the q-th diagonal element of $\mathbf{H}_1^{\mathcal{F}}$. Then, the achievable rate for the first user can be derived as

$$\begin{aligned}R_1^{\mathcal{F}} &= \frac{S_{\mathrm{f}}}{S_{\mathrm{f}}+N_{\mathrm{CP}}} \times G \times \frac{W}{S_{\mathrm{f}}} \times \mathcal{I}(\mathcal{X}^{\mathcal{C}}; \mathbf{y}_1^{\mathcal{F}}|\mathcal{X}^{\mathcal{F}}) \\ &= \frac{W S_{\mathrm{a}} S_{\mathrm{f}}}{S^2(S_{\mathrm{f}}+N_{\mathrm{CP}})} \sum_{q=1}^{S} \log_2\left(1+\frac{{H_{1,q}^{\mathcal{F}}}^2 PS}{S_{\mathrm{a}} N_0 W}\right).\end{aligned} \tag{44}$$

For the second user, the data information is conveyed by the frequency-domain symbols, the mutual information of which is given by

$$\begin{aligned}\mathcal{I}(\mathcal{X}^{\mathcal{F}}; \mathbf{y}_2^{\mathcal{F}}) =& \frac{1}{\binom{S}{S_{\mathrm{a}}}} \sum_{p=1}^{\binom{S}{S_{\mathrm{a}}}} \int_{\mathbf{y}_2^{\mathcal{F}}} f(\mathbf{y}_2^{\mathcal{F}}|\mathcal{X}^{\mathcal{F}} = \Phi_p) \times \\ & \log_2\left(\frac{f(\mathbf{y}_2^{\mathcal{F}}|\mathcal{X}^{\mathcal{F}} = \Phi_p)}{f(\mathbf{y}_2^{\mathcal{F}})}\right) \mathrm{d}\mathbf{y}_2^{\mathcal{F}},\end{aligned} \tag{45}$$

where $f(\mathbf{y}_2^{\mathcal{F}}|\mathcal{X}^{\mathcal{F}} = \Phi_p)$ and $f(\mathbf{y}_2^{\mathcal{F}})$ denote the conditional PDF and the PDF, respectively. Similar to the proof of *Proposition 1*, we can utilize the Jensen's inequality to derive the lower bound

$$I(\mathcal{X}^{\mathcal{F}}; \mathbf{y}_2^{\mathcal{F}}) \geq \log_2\left(\frac{\binom{S}{S_{\mathrm{a}}}}{e^S}\right) - \frac{1}{\binom{S}{S_{\mathrm{a}}}} \sum_{p=1}^{\binom{S}{S_{\mathrm{a}}}} \log_2\left(\sum_{r=1}^{\binom{S}{S_{\mathrm{a}}}} \frac{|\Sigma_p^{\mathcal{F}}|}{|\Sigma_p^{\mathcal{F}}+\Sigma_r^{\mathcal{F}}|}\right). \tag{46}$$

Thus, the lower bound of the achievable rate for the second

user can be expressed as

$$\begin{aligned} R_2^{\mathcal{F}} =& \frac{S_{\rm f}}{S_{\rm f}+N_{\rm CP}} \times G \times \frac{W}{S_{\rm f}} \times I(\mathcal{X}^{\mathcal{F}};\mathbf{y}_2^{\mathcal{F}}) \\ \geq& \frac{WS_{\rm f}}{S(S_{\rm f}+N_{\rm CP})}\log_2\left(\frac{\binom{S}{S_{\rm a}}}{e^S}\right) - \frac{WS_{\rm f}}{S(S_{\rm f}+N_{\rm CP})\binom{S}{S_{\rm a}}}\times \\ & \sum_{p=1}^{\binom{S}{S_{\rm a}}}\log_2\left(\sum_{r=1}^{\binom{S}{S_{\rm a}}}\frac{|\Sigma_p^{\mathcal{F}}|}{|\Sigma_p^{\mathcal{F}}+\Sigma_r^{\mathcal{F}}|}\right). \end{aligned} \tag{47}$$

Finally, the lower bound of the achievable sum rate can be derived by combining (44) and (47).

■

The approximation of the achievable sum rate can be further given in *Corollary 2*.

Corollary 2: In the FD-IDDMA scheme, the sum rate of the two users in one user cluster can be approximated as

$$\begin{aligned} R^{\mathcal{F}} \approx& \frac{WS_{\rm a}S_{\rm f}}{S^2(S_{\rm f}+N_{\rm CP})}\sum_{q=1}^{S}\log_2\left(1+\frac{{H_{1,q}^{\mathcal{F}}}^2 PS}{S_{\rm a}N_0W}\right) + \frac{WS_{\rm f}}{S(S_{\rm f}+N_{\rm CP})}\times \\ & \log_2\left(\frac{\binom{S}{S_{\rm a}}}{2^S}\right) - \frac{WS_{\rm f}}{S(S_{\rm f}+N_{\rm CP})\binom{S}{S_{\rm a}}}\sum_{p=1}^{\binom{S}{S_{\rm a}}}\log_2\left(\sum_{r=1}^{\binom{S}{S_{\rm a}}}\frac{|\Sigma_p^{\mathcal{F}}|}{|\Sigma_p^{\mathcal{F}}+\Sigma_r^{\mathcal{F}}|}\right). \end{aligned} \tag{48}$$

Proof: The result can be derived by applying a constant shift of $WS_{\rm f}\log_2(e/2)/(S_{\rm f}+N_{\rm CP})$ to (39) due to the limitation of (39) in low and high SNR regions. ■

Similarly, the lower bound of the achievable sum rate of the TD-IDDMA scheme can be obtained in *Proposition 3*.

Proposition 3: For a flat fading multi-user SISO communication system defined in Section III-A with T time slots in each frame, where the proposed TD-IDDMA is adopted with $T_{\rm a}$ time slots activated in each frame, the achievable sum rate for the two users in each user cluster can be lower bounded by

$$\begin{aligned} R^{\mathcal{T}} \geq& \frac{WT_{\rm a}}{T}\log_2\left(1+\frac{{h_1^{\mathcal{T}}}^2 P}{N_0W}\right) + \frac{W}{T}\log_2\left(\frac{\binom{T}{T_{\rm a}}}{e^T}\right) \\ & - \frac{W}{T\binom{T}{T_{\rm a}}}\sum_{p=1}^{\binom{T}{T_{\rm a}}}\log_2\left(\sum_{r=1}^{\binom{T}{T_{\rm a}}}\frac{|\Sigma_p^{\mathcal{T}}|}{|\Sigma_p^{\mathcal{T}}+\Sigma_r^{\mathcal{T}}|}\right), \end{aligned} \tag{49}$$

where W, P, and N_0 denote the bandwidth, the total transmit power, and the power density of the AWGN, respectively.

Proof: For the flat fading channel, the received signals in each frame by the two users U_k $(k=1,2)$ can be given by

$$\mathbf{y}_k^{\mathcal{T}} = h_k^{\mathcal{T}}\mathbf{x}^{\mathcal{T}} + \mathbf{w}_k^{\mathcal{T}}. \tag{50}$$

The total mutual information for the k-th user can be expressed as

$$\mathcal{I}(\mathbf{x}^{\mathcal{T}};\mathbf{y}_k^{\mathcal{T}}) = \mathcal{I}(\mathcal{X}^{\mathcal{C}},\mathcal{X}^{\mathcal{T}};\mathbf{y}_k^{\mathcal{T}}) = \mathcal{I}(\mathcal{X}^{\mathcal{C}};\mathbf{y}_k^{\mathcal{T}}|\mathcal{X}^{\mathcal{T}}) + \mathcal{I}(\mathcal{X}^{\mathcal{T}};\mathbf{y}_k^{\mathcal{T}}), \tag{51}$$

where $\mathcal{I}(\mathcal{X}^{\mathcal{C}};\mathbf{y}_k^{\mathcal{T}}|\mathcal{X}^{\mathcal{T}})$ and $\mathcal{I}(\mathcal{X}^{\mathcal{T}};\mathbf{y}_k^{\mathcal{T}})$ represent the mutual information conveyed by the constellation-domain symbols and time-domain symbols, respectively. For the first user desiring constellation-domain symbols, the achievable rate can be given by

$$R_1^{\mathcal{T}} = \frac{WT_{\rm a}}{T}\log_2\left(1+\frac{{h_1^{\mathcal{T}}}^2 P}{N_0W}\right). \tag{52}$$

For the second user, the data information is conveyed by the time-domain symbols, the mutual information of which is given by

$$\begin{aligned} \mathcal{I}(\mathcal{X}^{\mathcal{T}};\mathbf{y}_2^{\mathcal{T}}) =& \frac{1}{\binom{T}{T_{\rm a}}}\sum_{p=1}^{\binom{T}{T_{\rm a}}}\int_{\mathbf{y}_2^{\mathcal{T}}} f(\mathbf{y}_2^{\mathcal{T}}|\mathcal{X}^{\mathcal{T}}=\Theta_p)\times \\ & \log_2\left(\frac{f(\mathbf{y}_2^{\mathcal{T}}|\mathcal{X}^{\mathcal{T}}=\Theta_p)}{f(\mathbf{y}_2^{\mathcal{T}})}\right)\mathrm{d}\mathbf{y}_2^{\mathcal{T}}, \end{aligned} \tag{53}$$

where $f(\mathbf{y}_2^{\mathcal{T}}|\mathcal{X}^{\mathcal{T}}=\Theta_p)$ and $f(\mathbf{y}_2^{\mathcal{T}})$ denote the conditional PDF and the PDF, respectively. Similar to the proof of *Proposition 1*, we can utilize the Jensen's inequality to derive the lower bound of the achievable rate for the second user

$$R_2^{\mathcal{T}} \geq \frac{W}{T}\log_2\left(\frac{\binom{T}{T_{\rm a}}}{e^T}\right) - \frac{W}{T\binom{T}{T_{\rm a}}}\sum_{p=1}^{\binom{T}{T_{\rm a}}}\log_2\left(\sum_{r=1}^{\binom{T}{T_{\rm a}}}\frac{|\Sigma_p^{\mathcal{T}}|}{|\Sigma_p^{\mathcal{T}}+\Sigma_r^{\mathcal{T}}|}\right). \tag{54}$$

Finally, the lower bound of the achievable sum rate can be derived by combining (52) and (54).

■

In the end, the approximation can be further given in *Corollary 3*.

Corollary 3: In the TD-IDDMA scheme, the sum rate of the two users in one user cluster can be approximated as

$$\begin{aligned} R^{\mathcal{T}} \approx& \frac{WT_{\rm a}}{T}\log_2\left(1+\frac{{h_1^{\mathcal{T}}}^2 P}{N_0W}\right) + \frac{W}{T}\log_2\left(\frac{\binom{T}{T_{\rm a}}}{2^T}\right) \\ & - \frac{W}{T\binom{T}{T_{\rm a}}}\sum_{p=1}^{\binom{T}{T_{\rm a}}}\log_2\left(\sum_{r=1}^{\binom{T}{T_{\rm a}}}\frac{|\Sigma_p^{\mathcal{T}}|}{|\Sigma_p^{\mathcal{T}}+\Sigma_r^{\mathcal{T}}|}\right). \end{aligned} \tag{55}$$

Proof: The result can be derived by applying a constant shift of $W\log_2(e/2)$ to (49) due to the limitation of (49) in low and high SNR regions. ■

B. Computational Complexity Analyses

In this subsection, the computational complexity of the proposed detection method is analyzed. Similar to [36] and [37], the total number of real floating-point operations (flops) are investigated. We consider a communication system using IDDMA with four users supported in each user cluster.

For user U_4, the calculation of the Frobenius norm of $\dot{\mathbf{Y}}_4^{(t)}$ in one time block contains $(4M_4S_{\rm f}-1)$ flops. Selecting $T_{\rm a}$ from T time blocks contains T^2 flops at most. Therefore, the average complexity for U_4 detecting the signals in one time block contains $(T(4M_4S_{\rm f}-1)+T^2)/T = (4M_4S_{\rm f}-1+T)$ flops.

For user U_3, the ZF equalizer contains $NS_{\rm f}(8M_3-2)$ flops. The calculation of the Frobenius norm of N rows in $\hat{\mathbf{X}}^{(t)}$ contains $N(4S_{\rm f}-1)$ flops. Selecting $N_{\rm a}$ rows with the largest

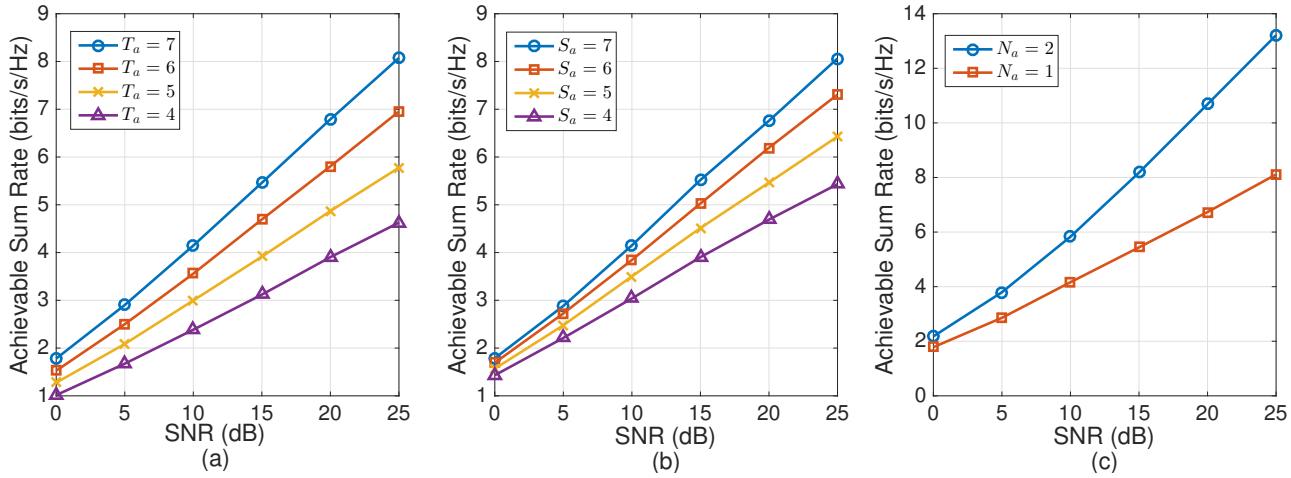


Fig. 5. Achievable sum rate comparison of the proposed IDDMA scheme under different conditions: a) different numbers of activated time blocks T_{a}; b) different numbers of activated subcarriers S_{a}; c) different numbers of activated transmit antennas N_{a}.

Frobenius norm contains N^2 flops at most. Comparison with the threshold η_3 contains N_{a} flops. Thus, the total complexity for U_3 is $(8NM_3S_{\mathrm{f}} + 2NS_{\mathrm{f}} + N^2 - N + N_a)$ for detecting the signals in one time block.

For user U_2, the FFT operation and ZF equalizer contain $5M_2S_{\mathrm{f}}\log_2(S_{\mathrm{f}})$ and $NS_{\mathrm{f}}(8M_2 - 2)$ flops, respectively. For each row of $\hat{\mathbf{X}}^{(t)}$, selecting the activated subcarriers and comparing with η_2 contain $(G(3S+S^2)+GS_{\mathrm{a}})$ flops in total. As a result, the total complexity for U_2 is $(5M_2S_{\mathrm{f}}\log_2(S_{\mathrm{f}}) + 8M_2NS_{\mathrm{f}} + NS_{\mathrm{f}}S + NGS_{\mathrm{a}} + NS_{\mathrm{f}})$.

For user U_1, the ML detection method can achieve optimal detection performance. However, the complexity is extremely high. For detecting the constellation-domain symbols in one time block, the search space is given by $\mathcal{O}((Q+1)^{NS_{\mathrm{f}}})$. The sphere decoding based methods [38], [39] and the compressive sensing based methods [40], [36] can be used to reduce the detection complexity for U_1.

VI. Simulation Results and Discussions

In this section, we provide simulation results and discussions of the proposed IDDMA scheme. The achievable rate, detection complexity, BER performance and special cases of the proposed scheme are investigated in Section VI-A, Section VI-B, Section VI-C and Section VI-D, respectively. We consider a multi-user communication system supporting four users in each user cluster, where U_1 is a smart electronic device, while U_2, U_3 and U_4 are IoT devices. At the base station, $N = 2$ transmit antennas are utilized to support this user cluster, and each user is equipped with $M_k = 2$ receive antennas. The whole bandwidth is divided into $S_{\mathrm{f}} = 64$ subcarriers, which are further grouped into $G = 8$ subcarrier groups with $S = S_{\mathrm{f}}/G = 8$ subcarriers in each group. Each frame contains $T = 8$ time blocks and the Rayleigh flat fading channel is considered for each time block. The information bits for different users are conveyed by the constellation-, frequency-, spatial-, and time-domain symbols, respectively, as explained in Section IV. The default numbers of the activated resources are $T_{\mathrm{a}} = 7$, $S_{\mathrm{a}} = 7$, and $N_{\mathrm{a}} = 1$, unless particularly stated.

A. Achievable Rate

Firstly, we analyze the achievable rate of the proposed IDDMA scheme. The achievable sum rate under different conditions is provided in Fig. 5 through Monte-Carlo method. The achievable sum rates with different numbers of activated resources T_{a}, S_{a}, and N_{a} are illustrated in Fig. 5(a), Fig. 5(b), and Fig. 5(c), respectively. It can be seen that the achievable sum rates increase with the rise of SNR under each condition. It can also be seen that the achievable sum rates increase with the rise of the numbers of activated resources T_{a}, S_{a}, and N_{a}. This is mainly because that more degrees of freedom are available for data modulation by activating more resources. It can be seen that the gaps between the lines in Fig. 5(a), Fig. 5(b), and Fig. 5(c) are different, which shows that the number of activated time blocks T_{a}, subcarriers S_{a}, and transmit antennas N_{a} have different impacts on the achievable sum rates of the system. Therefore, flexible multiple access can be employed by adjusting the numbers of activated resources according to the requirements of the users.

B. Detection Complexity

We further investigate the computational complexity of the proposed detection method in this section. We consider a similar multi-user communication system as Section VI-A. The system parameters are the same as Section VI-A, except that only one receive antenna is equipped at each user. We also simulate the detection complexity of the conventional OFDM-NOMA system [41] as comparison, which overlaps the signals with diverse power levels for different users on each subcarrier. The SIC detection method using ZF equalizer is adopted for OFDM-NOMA. The simulated computational complexity for the IoT users U_2, U_3, U_4 is illustrated in Fig. 6, where 4QAM modulation is considered and the common complexity caused by FFT is omitted. We use different colors to indicate

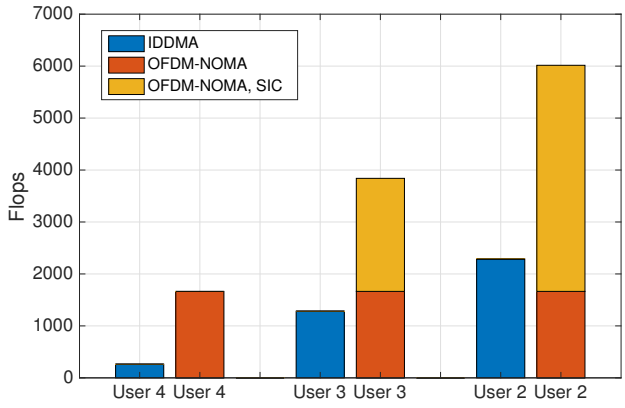


Fig. 6. Complexity comparison of the proposed IDDMA scheme and the conventional OFDM-NOMA scheme.

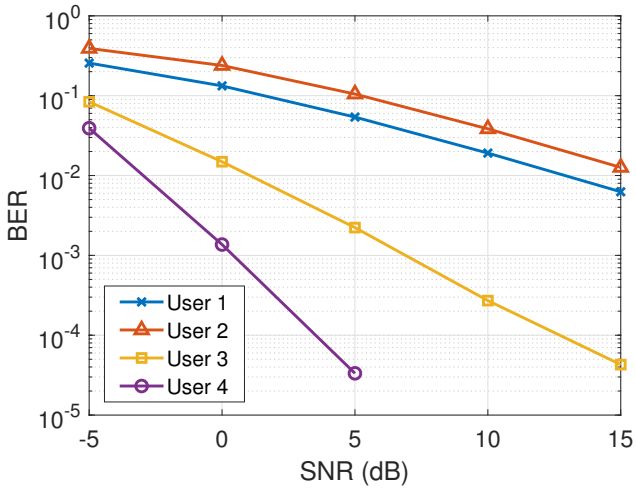


Fig. 7. BER performance of the proposed IDDMA scheme.

the computational complexity caused by decoding the desired information and the SIC in OFDM-NOMA. It can be seen that the proposed IDDMA scheme enjoys much less detection complexity than the conventional OFDM-NOMA scheme. This is mainly because that in the proposed scheme, the SIC is avoided by modulating information for different users on different domains of the signals. Moreover, the detection of the indices of the activated resources in IDDMA involves much less complexity than the detection of the APM symbols in conventional OFDM-NOMA.

C. BER Performance

In this subsection, we investigate the BER performance of the proposed IDDMA scheme. The system parameters are the same as those in Section VI-A. In the simulation, the proposed low-complexity MRC-based detection method is used. For U_2 and U_3, the MMSE equalizers are adopted. For U_1, the two-step detection method is used to decrease complexity. The simulation results are given in Fig. 7, where 4QAM modulation is considered. It can be seen that the BER performances of the users are different. U_4 enjoys the lowest BER. U_3 exhibits higher BER than U_4, which is mainly because the MMSE equalizer cannot cancel the interference from the transmit antennas completely. U_2 and U_1 have the worst BER performances. This is mainly because the FFT process is applied to recover the frequency-domain signals, which spreads errors and make it difficult for the users to detect the indices of the activated subcarriers and the APM symbols.

The MRC-based detection methods used in this paper can serve as benchmarks for future research. Other detection methods for IM, including sphere decoding based methods [38], [39], compressive sensing based methods [40], [36], and log-likelihood ratio based methods [42], [43], can also be used to improve the detection performance, while more complexity will be expected.

D. Special Cases

The special cases explained in Section IV-C are important components of the proposed IDDMA framework and can be easily employed in the current and future wireless communication systems. In this section, we investigate the performance of the special cases TD-IDDMA, FD-IDDMA, and SD-IDDMA when applied to SISO systems, OFDM systems, and MIMO systems, respectively. The detailed simulation parameters are provided in Table I. Two users are supported in each user cluster. In conventional power-domain NOMA schemes, 8 dB difference in propagation loss is required for user pairing [11]. Therefore, the propagation loss of U_2 is set to be 8 dB worse than U_1 in the simulation. The accuracy of the proposed approximations and lower bounds of the achievable sum rate is investigated in Fig. 8. The exact values through Monte-Carlo method, the proposed approximations, and the derived lower bounds are illustrated as solid lines, dotted lines, and dash-dotted lines, respectively. It can be seen that the lower bounds can track the trends of the exact values very well. And the further proposed approximations are very close to the exact values under all the simulated situations, which proves that the proposed approximations can be used to calculate the achievable sum rate efficiently with high accuracy.

In Fig. 9, we further compare the achievable sum rate of the proposed scheme with conventional NOMA schemes [10] and orthogonal frequency division multiple access (OFDMA) schemes. In the proposed scheme, the numbers of activated resources are $T_{\mathrm{a}} = 7$, $S_{\mathrm{a}} = 7$, and $N_{\mathrm{a}} = 3$ for TD-IDDMA, FD-IDDMA, and SD-IDDMA, respectively. In the conventional NOMA schemes, the information for the two users are transmitted with different power. αP is allocated to U_1, and $(1-\alpha)P$ is allocated to U_2, respectively. The first user utilizes SIC to remove the interference caused by the second user. In practical system, the imperfection of SIC has a great impact on the performance [44]. Thus, we use ϵ to denote the cancellation error term [45] that represents the remaining portion of the canceled signals by SIC. In the OFDMA scheme, we allocate βP power and γW bandwidth to U_1, and $(1-\beta)P$ power and $(1-\gamma)W$ bandwidth to U_2. The simulation results are shown in Fig. 9 with $\alpha = 0.2$, $\beta = 0.7$ and $\gamma = 0.7$. It can be seen that the proposed schemes can

TABLE I
SIMULATION PARAMETERS

Systems	SISO System	OFDM System	MIMO System
Transmit Antennas	$N = 1$	$N = 1$	$N = 4$
Receive Antennas	$M_1 = M_2 = 1$	$M_1 = M_2 = 1$	$M_1 = M_2 = 4$
Time Slots	$T = 8$	/	/
Subcarriers	/	$S_{\mathrm{f}} = 64,\ G = 8$	/

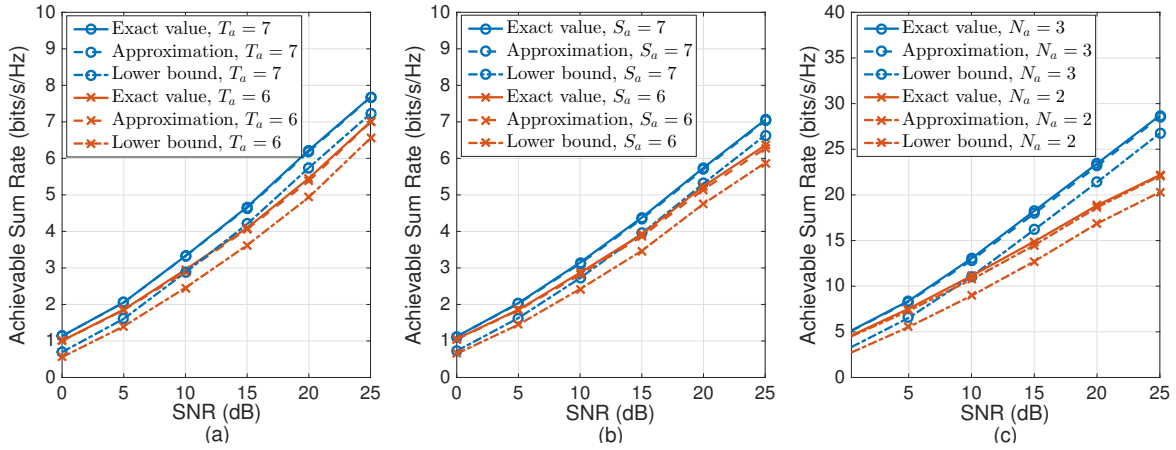


Fig. 8. Achievable sum rate comparison of the exact values, approximations, and lower bounds for the special cases of the proposed IDDMA schemes: a) the TD-IDDMA scheme; b) the FD-IDDMA scheme; c) the SD-IDDMA scheme.

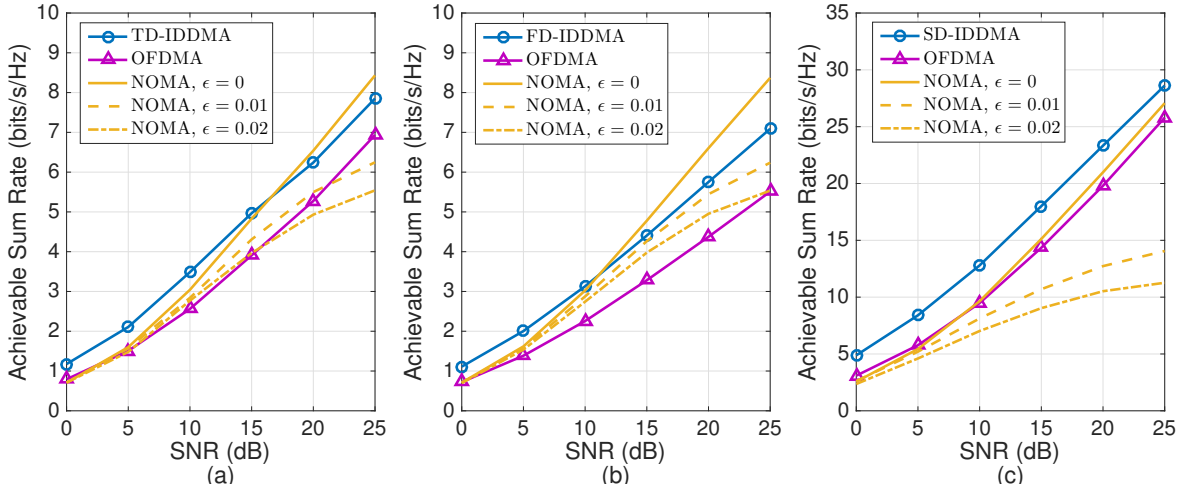


Fig. 9. Achievable sum rate comparison of the proposed schemes, conventional NOMA schemes, and conventional OMA schemes: a) the TD-IDDMA scheme; b) the FD-IDDMA scheme; c) the SD-IDDMA scheme.

achieve better performance than the OFDMA schemes, which is mainly because of the alleviated interference. It can also be seen that in Fig. 9(a) and Fig. 9(b), the proposed schemes can achieve similar performance with the NOMA schemes from low to medium SNR regions with perfect SIC. However, the performance of conventional NOMA decreases a lot even with slightly imperfect SIC. It can be seen that the proposed schemes obtain much higher sum rates than the NOMA schemes with $\epsilon = 0.01$ and $\epsilon = 0.02$. In the MIMO system shown in Fig. 9(c), the proposed scheme outperforms the conventional NOMA scheme even with perfect SIC detection. This is mainly because that the intra-cluster interference is increased with more transmit antennas in conventional NOMA schemes, which is alleviated in the proposed scheme.

VII. CONCLUSION

In this paper, a novel IDDMA scheme has been proposed for the beyond 5G wireless communication systems, which builds a framework based on the principle of the multi-domain IM to enable flexible multiple access between the two kinds

of key users in the future wireless communication systems, namely, the smart electronic devices and the IoT devices. Due to multi-domain consideration and manipulation, the intra-cluster interference is alleviated and the complicated SIC is avoided at the user side. The achievable rate of the proposed scheme has been analyzed and a closed-form approximation of the achievable sum rate has been derived. The superior performance compared with the conventional multiple access schemes are validated through numerical simulations. The proposed scheme and its special cases can be easily deployed in the widely used wireless communication systems, including the multi-user MIMO systems and the multi-user OFDM systems.

REFERENCES

[1] A. Zanella, N. Bui, A. Castellani, L. Vangelista, and M. Zorzi, "Internet of Things for smart cities," *IEEE Internet Things J.*, vol. 1, no. 1, pp. 22–32, Feb. 2014.

[2] T. Jiang, H. Fang, and H. Wang, "Blockchain-based Internet of Vehicles: Distributed network architecture and performance analysis," *IEEE Internet Things J.*, vol. 6, no. 3, pp. 4640–4649, Jun. 2019.

[3] T. Wang, J. Tan, W. Ding, Y. Zhang, F. Yang, J. Song, and Z. Han, "Intercommunity detection scheme for social Internet of Things: Compressive sensing over graphs approach," *IEEE Internet Things J.*, vol. 5, no. 6, pp. 4550–4557, Dec. 2018.

[4] G. A. Akpakwu, B. J. Silva, G. P. Hancke, and A. M. Abu-Mahfouz, "A survey on 5G networks for the Internet of Things: Communication technologies and challenges," *IEEE Access*, vol. 6, pp. 3619–3647, Feb. 2018.

[5] Q. Qi, X. Chen, and D. W. K. Ng, "Robust beamforming for NOMA-based cellular massive IoT with SWIPT," *IEEE Trans. Signal Process.*, vol. 68, no. 15, pp. 211–224, Dec. 2019.

[6] M. Shafi, A. F. Molisch, P. J. Smith, T. Haustein, P. Zhu, P. De Silva, F. Tufvesson, A. Benjebbour, and G. Wunder, "5G: A tutorial overview of standards, trials, challenges, deployment, and practice," *IEEE J. Sel. Areas Commun.*, vol. 35, no. 6, pp. 1201–1221, Jun. 2017.

[7] W. Saad, M. Bennis, and M. Chen, "A vision of 6G wireless systems: Applications, trends, technologies, and open research problems," *IEEE Netw.*, vol. 34, no. 3, pp. 134–142, May 2020.

[8] B. Mao, Y. Kawamoto, and N. Kato, "AI-based joint optimization of QoS and security for 6G energy harvesting Internet of Things," *IEEE Internet Things J.*, vol. 7, no. 8, pp. 7032–7042, Aug. 2020.

[9] T. Mao, Q. Wang, Z. Wang, and S. Chen, "Novel index modulation techniques: A survey," *IEEE Commun. Surveys Tuts.*, vol. 21, no. 1, pp. 315–348, Jul. 2019.

[10] Z. Ding, X. Lei, G. K. Karagiannidis, R. Schober, J. Yuan, and V. K. Bhargava, "A survey on non-orthogonal multiple access for 5G networks: Research challenges and future trends," *IEEE J. Sel. Areas Commun.*, vol. 35, no. 10, pp. 2181–2195, Oct. 2017.

[11] S. M. R. Islam, N. Avazov, O. A. Dobre, and K. Kwak, "Power-domain non-orthogonal multiple access (NOMA) in 5G systems: Potentials and challenges," *IEEE Commun. Surveys Tuts.*, vol. 19, no. 2, pp. 721–742, May 2017.

[12] R. Hoshyar, F. P. Wathan, and R. Tafazolli, "Novel low-density signature for synchronous CDMA systems over AWGN channel," *IEEE Trans. Signal Process.*, vol. 56, no. 4, pp. 1616–1626, Apr. 2008.

[13] H. Nikopour and H. Baligh, "Sparse code multiple access," in *IEEE 24th Annual International Symposium on Personal, Indoor, and Mobile Radio Communications (PIMRC)*, London, United Kingdom, Sep. 2013, pp. 332–336.

[14] M. Nakao, T. Ishihara, and S. Sugiura, "Single-carrier frequency-domain equalization with index modulation," *IEEE Commun. Lett.*, vol. 21, no. 2, pp. 298–301, Feb. 2017.

[15] M. Nakao and S. Sugiura, "Dual-mode time-domain single-carrier index modulation with frequency-domain equalization," in *IEEE 86th Vehicular Technology Conference (VTC Fall)*, Toronto, Canada, Sep. 2017.

[16] M. Wen, B. Zheng, K. J. Kim, M. D. Renzo, T. A. Tsiftsis, K. Chen, and N. Al-Dhahir, "A survey on spatial modulation in emerging wireless systems: Research progresses and applications," *IEEE J. Sel. Areas Commun.*, vol. 37, no. 9, pp. 1949–1972, Sep. 2019.

[17] M. D. Renzo, H. Haas, A. Ghrayeb, S. Sugiura, and L. Hanzo, "Spatial modulation for generalized MIMO: Challenges, opportunities, and implementation," *Proc. IEEE*, vol. 102, no. 1, pp. 56–103, Jan. 2014.

[18] E. Basar, M. Wen, R. Mesleh, M. D. Renzo, Y. Xiao, and H. Haas, "Index modulation techniques for next-generation wireless networks," *IEEE Access*, vol. 5, pp. 16 693–16 746, Aug. 2017.

[19] E. Basar, "Index modulation techniques for 5G wireless networks," *IEEE Commun. Mag.*, vol. 54, no. 7, pp. 168–175, Jul. 2016.

[20] L. He, J. Wang, and J. Song, "Spatial modulation for more spatial multiplexing: RF-chain-limited generalized spatial modulation aided mm-Wave MIMO with hybrid precoding," *IEEE Trans. Commun.*, vol. 66, no. 3, pp. 986–998, Mar. 2018.

[21] Y. Cui and X. Fang, "Performance analysis of massive spatial modulation MIMO in high-speed railway," *IEEE Trans. Veh. Technol.*, vol. 65, no. 11, pp. 8925–8932, Nov. 2016.

[22] T. Wang, F. Yang, J. Song, and Z. Han, "Dimming techniques of visible light communications for human-centric illumination network: State-of-the-art, challenges, and trends," *IEEE Wireless Commun.*, vol. 27, no. 4, pp. 88–95, Aug. 2020.

[23] X. Zhu, Z. Wang, and J. Cao, "NOMA-based spatial modulation," *IEEE Access*, vol. 5, pp. 3790–3800, Mar. 2017.

[24] X. Wang, J. Wang, L. He, Z. Tang, and J. Song, "On the achievable spectral efficiency of spatial modulation aided downlink non-orthogonal multiple access," *IEEE Commun. Lett.*, vol. 21, no. 9, pp. 1937–1940, Sep. 2017.

[25] P. Yang, Y. Xiao, M. Xiao, and Z. Ma, "NOMA-aided precoded spatial modulation for downlink MIMO transmissions," *IEEE J. Sel. Topics Signal Process.*, vol. 13, no. 3, pp. 729–738, Jun. 2019.

[26] C. Zhong, X. Hu, X. Chen, D. W. K. Ng, and Z. Zhang, "Spatial modulation assisted multi-antenna non-orthogonal multiple access," *IEEE Wireless Commun.*, vol. 25, no. 2, pp. 61–67, Apr. 2018.

[27] Q. Li, M. Wen, E. Basar, H. V. Poor, and F. Chen, "Spatial modulation-aided cooperative NOMA: Performance analysis and comparative study," *IEEE J. Sel. Topics Signal Process.*, vol. 13, no. 3, pp. 715–728, Jun. 2019.

[28] T. Wang, F. Yang, and J. Song, "Novel index modulation aided non-orthogonal multiple access for visible light communication," in *IEEE Global Communications Conference (GLOBECOM)*, Waikoloa, HI, Dec. 2019.

[29] Q. Li, G. Li, W. Lee, M. Lee, D. Mazzarese, B. Clerckx, and Z. Li, "MIMO techniques in WiMAX and LTE: a feature overview," *IEEE Commun. Mag.*, vol. 48, no. 5, pp. 86–92, May 2010.

[30] T. Hwang, C. Yang, G. Wu, S. Li, and G. Ye Li, "OFDM and its wireless applications: A survey," *IEEE Trans. Veh. Technol.*, vol. 58, no. 4, pp. 1673–1694, May 2009.

[31] A. Ghosh, R. Ratasuk, B. Mondal, N. Mangalvedhe, and T. Thomas, "LTE-advanced: next-generation wireless broadband technology," *IEEE Wireless Commun.*, vol. 17, no. 3, pp. 10–22, Jun. 2010.

[32] M. S. Ali, H. Tabassum, and E. Hossain, "Dynamic user clustering and power allocation for uplink and downlink non-orthogonal multiple access (NOMA) systems," *IEEE Access*, vol. 4, pp. 6325–6343, Aug. 2016.

[33] Z. Ding, P. Fan, and H. V. Poor, "Impact of user pairing on 5G nonorthogonal multiple-access downlink transmissions," *IEEE Trans. Veh. Technol.*, vol. 65, no. 8, pp. 6010–6023, Aug. 2016.

[34] J. Fu, C. Hou, W. Xiang, L. Yan, and Y. Hou, "Generalised spatial modulation with multiple active transmit antennas," in *IEEE Global Communications Conference Workshops (GLOBECOM Workshops)*, Miami, FL, Dec. 2010, pp. 839–844.

[35] Z. An, J. Wang, J. Wang, and J. Song, "Mutual information and error probability analysis on generalized spatial modulation system," *IEEE Trans. Commun.*, vol. 65, no. 3, pp. 1044–1060, Mar. 2017.

[36] T. Wang, S. Liu, F. Yang, J. Wang, J. Song, and Z. Han, "Generalized spatial modulation-based multi-user and signal detection scheme for terrestrial return channel with NOMA," *IEEE Trans. Broadcast.*, vol. 64, no. 2, pp. 211–219, Jun. 2018.

[37] Y. Xiao, Z. Yang, L. Dan, P. Yang, L. Yin, and W. Xiang, "Low-complexity signal detection for generalized spatial modulation," *IEEE Commun. Lett.*, vol. 18, no. 3, pp. 403–406, Mar. 2014.

[38] A. Younis, S. Sinanovic, M. Di Renzo, R. Mesleh, and H. Haas, "Generalised sphere decoding for spatial modulation," *IEEE Trans. Commun.*, vol. 61, no. 7, pp. 2805–2815, Jul. 2013.

[39] J. A. Cal-Braz and R. Sampaio-Neto, "Low-complexity sphere decoding detector for generalized spatial modulation systems," *IEEE Commun. Lett.*, vol. 18, no. 6, pp. 949–952, Jun. 2014.

[40] L. Xiao, P. Yang, Y. Xiao, S. Fan, M. Di Renzo, W. Xiang, and S. Li, "Efficient compressive sensing detectors for generalized spatial modulation systems," *IEEE Trans. Veh. Technol.*, vol. 66, no. 2, pp. 1284–1298, Feb. 2017.
[41] X. Li, C. Li, and Y. Jin, "Dynamic resource allocation for transmit power minimization in OFDM-based NOMA systems," *IEEE Commun. Lett.*, vol. 20, no. 12, pp. 2558–2561, Dec. 2016.
[42] E. Basar, U. Aygolu, E. Panayirci, and H. V. Poor, "Orthogonal frequency division multiplexing with index modulation," *IEEE Trans. Signal Process.*, vol. 61, no. 22, pp. 5536–5549, Nov. 2013.
[43] T. Mao, Z. Wang, Q. Wang, S. Chen, and L. Hanzo, "Dual-mode index modulation aided OFDM," *IEEE Access*, vol. 5, pp. 50–60, Aug. 2016.
[44] X. Chen, R. Jia, and D. W. K. Ng, "On the design of massive non-orthogonal multiple access with imperfect successive interference cancellation," *IEEE Trans. Commun.*, vol. 67, no. 3, pp. 2539–2551, Mar. 2019.
[45] J. G. Andrews and T. H. Meng, "Optimum power control for successive interference cancellation with imperfect channel estimation," *IEEE Trans. Wireless Commun.*, vol. 2, no. 2, pp. 375–383, Mar. 2003.



Tengjiao Wang (S'19) received his B.S. degree from the Department of Electronic Engineering, Tsinghua University, Beijing, China, in 2016. He is currently pursuing the Ph.D. degree with the DTV Technology Research and Development Center, Department of Electronic Engineering, Tsinghua University. He was a Visiting Student with Massachusetts Institute of Technology, Cambridge, MA, USA in 2019. His research interests lie in the fields of wireless communications, visible light communications, Internet of Things, and machine learning. He was a recipient of the National Scholarship in 2018 and the Academic Star of Electronic Engineering Department, Tsinghua University in 2019.



Fang Yang (M'11-SM'13) received the B.S.E. and Ph.D. degrees in electronic engineering from Tsinghua University, Beijing, China, in 2005 and 2009, respectively. He is currently working as an Associate Professor with the Research Institute of Information Technology, Tsinghua University. He has published over 120 peer-reviewed journal and conference papers. He holds over 40 Chinese patents and 2 PCT patents. His research interests lie in the fields of channel coding, channel estimation, interference cancellation, and signal processing techniques for communication system, especially in power line communication, visible light communication, and digital television terrestrial broadcasting. Dr. Yang received the IEEE Scott Helt Memorial Award (best paper award in IEEE Transactions in Broadcasting) in 2015. He is the Secretary General of Sub-Committee 25 of the China National Information Technology Standardization (SAC/TC28/SC25), and a fellow of IET.



Changyong Pan (M'05-SM'12) received his B. Eng and M . Eng. degrees in Electrical Engineering both from Tsinghua University, Beijing China in 1996 and 1998, respectively and worked for the same university upon his graduation. He is a full professor in the Research Institute of information technology of Tsinghua University. He has authored or co-authored more than 180 technical papers and published 8 technical book. He holds 34 patents, won national technical award three times and is also the winner of numerous other awards. He is Fellow of both IET and CIE.



Jian Song (M'06-SM'10-F'16) received his B. Eng and Ph. D. degrees in Electrical Engineering both from Tsinghua University, Beijing, China in 1990 and 1995, respectively and worked for the same university upon his graduation. He has worked at The Chinese University of Hong Kong and University of Waterloo, Canada in 1996 and 1997, respectively. He has been with Hughes Network Systems in USA for 7 years before joining the faculty team in Tsinghua in 2005 as a professor. He is now the director of Tsinghua's DTV Technology R&D center. He has been working in quite different areas of fiber-optic, satellite, wireless communications and the power line communications. His current research interest is in the area of digital TV broadcasting. He has published more than 270 peer-reviewed journal and conference papers. He holds 2 US and more than 70 Chinese patents. He is also Fellow of IET.



Zhu Han (S'01-M'04-SM'09-F'14) received the B.S. degree in electronic engineering from Tsinghua University, in 1997, and the M.S. and Ph.D. degrees in electrical and computer engineering from the University of Maryland, College Park, in 1999 and 2003, respectively.

From 2000 to 2002, he was an R&D Engineer of JDSU, Germantown, Maryland. From 2003 to 2006, he was a Research Associate at the University of Maryland. From 2006 to 2008, he was an assistant professor at Boise State University, Idaho. Currently, he is a John and Rebecca Moores Professor in the Electrical and Computer Engineering Department as well as in the Computer Science Department at the University of Houston, Texas. His research interests include wireless resource allocation and management, wireless communications and networking, game theory, big data analysis, security, and smart grid. Dr. Han received an NSF Career Award in 2010, the Fred W. Ellersick Prize of the IEEE Communication Society in 2011, the EURASIP Best Paper Award for the Journal on Advances in Signal Processing in 2015, IEEE Leonard G. Abraham Prize in the field of Communications Systems (best paper award in IEEE JSAC) in 2016, and several best paper awards in IEEE conferences. Dr. Han was an IEEE Communications Society Distinguished Lecturer from 2015-2018, AAAS fellow since 2019 and ACM distinguished Member since 2019. Dr. Han is 1% highly cited researcher since 2017 according to Web of Science. Dr. Han is also the winner of 2021 IEEE Kiyo Tomiyasu Award, for outstanding early to mid-career contributions to technologies holding the promise of innovative applications, with the following citation: "for contributions to game theory and distributed management of autonomous communication networks."